arXiv:2001.07647v1 [nlin.PS] 21 Jan 2020

Modulation theory and resonant regimes for dispersive shock waves in nematic liquid crystals

Saleh Baqer,
School of Mathematics, University of Edinburgh,
Edinburgh, Scotland, EH9 3FD, U.K.

Noel F. Smyth,
School of Mathematics, University of Edinburgh,
Edinburgh, Scotland, EH9 3FD, U.K. and
School of Mathematics and Applied Statistics, University of Wollongong,
Northfields Avenue, Wollongong, N.S.W., Australia, 2522.

Abstract

A full analysis of all regimes for optical dispersive shock wave (DSW) propagation in nematic liquid crystals is undertaken. These dispersive shock waves are generated from step initial conditions for the optical field and are resonant in that linear diffractive waves are in resonance with the DSW, resulting in a resonant linear wavetrain propagating ahead of it. It is found that there are six regimes, which are distinct and require different solution methods. In previous studies, the same solution method was used for all regimes, which does not yield solutions in full agreement with numerical solutions. Indeed, the standard DSW structure disappears for sufficiently large initial jumps. Asymptotic theory, approximate methods or Whitham modulation theory are used to find solutions for these resonant dispersive shock waves in a given regime. The solutions are found to be in excellent agreement with numerical solutions of the nematic equations in all regimes. It is found that for small initial jumps, the resonant wavetrain is unstable, but that it stabilises above a critical jump height. It is additionally found that the DSW is unstable, except for small jump heights for which there is no resonance and large jump heights for which there is no standard DSW structure.

1 Introduction

The generic solutions of nonlinear, dispersive wave equations, such as the Korteweg-de Vries (KdV) and nonlinear Schrödinger (NLS) equations, are the solitary wave, soliton for integrable equations, and the dispersive shock wave (DSW), also termed an undular bore in fluid mechanics applications. Of these, the solitary wave (soliton) is the most widely studied [1, 2] as it is a steady solution, so that its solution is given by an ordinary differential equation, rather than the original full, dispersive, nonlinear partial differential equation. In addition, for integrable equations, solitons naturally arise from the point spectrum of the associated scattering problem [1, 2]. In general, a DSW is a modulated wavetrain which links two distinct states in a smooth manner, in contrast to a compressible flow shock, which is a discontinuous jump between two flow states [1]. It should be noted that in fluid mechanics, bores come in two general forms, viscous bores and undular bores [3]. A viscous bore is a steady wave

form due to a balance between viscosity and dispersion/nonlinearity, so that viscous bores dissipate energy [1, 3, 4]. In contrast, for a DSW, an undular bore in fluid mechanics, there is no loss and it is an unsteady, continually expanding, modulated wave for which dispersion stops nonlinear breaking, as occurs for a gas dynamic shock. In its standard form, a DSW is a modulated periodic wavetrain, with solitary waves at one edge and linear dispersive waves at the other [3], the classic example being the KdV DSW. DSWs arise in a wide range of applications, including meteorology [5, 6, 7], oceanography [8, 9], water waves [9, 10], geophysics [11, 12, 13, 14], nonlinear optics [15, 16, 17, 18], Bose-Einstein condensates [19], Fermionic fluids [20] and colloidal media [21], see [3] for a summary and appreciation of these applications.

The unsteady nature of a DSW meant that the study of these wave forms fell behind that of solitary waves (solitons). The breakthrough in their study came from the development of Whitham modulation theory [1, 22, 23], also termed the method of averaged Lagrangians. Whitham modulation theory is a powerful method to analyse slowly varying linear, and importantly, nonlinear, periodic dispersive waves. It is related to the general method of multiple scales [1]. Whitham modulation theory generates so-called modulation equations for the parameters , such as amplitude, wavenumber and mean height, describing a modulated (slowly) varying wavetrain. If these modulation equations are hyperbolic, the underlying nonlinear periodic wave is stable and if they are elliptic, the wave is unstable. Whitham used modulation theory to give a theoretical explanation of the Benjamin-Feir instability of gravity water waves [1, 24], showing that the modulation equations for these waves are elliptic if the product kh of the depth of the water h and the wavenumber k is above a critical value. The breakthrough for the theory of DSWs was the realisation that if the modulation equations for a nonlinear, dispersive wave equation form a hyperbolic system, then a simple wave solution of these equations corresponds to a DSW, the first DSW solution being that for the KdV equation [25] based on its previously derived modulation equations [1, 23]. The original derivation of the KdV modulation equations [1, 23] relied on extensive manipulation of what are essentially elliptic integrals as the periodic wave solution of the KdV equation is given in terms of the Jacobian elliptic cosine function $\mathrm{cn}\, z$. The KdV equation is the standard example of an equation which is exactly integrable via the method of inverse scattering [1, 2]. Using techniques from functional analysis, it was found that this spectral solution could be used to immediately determine the modulation equations for the KdV equation [26], with the methods applicable to any integrable nonlinear, dispersive wave equation.

In principle, the DSW solution for any nonlinear, dispersive wave equation with a modulationally stable periodic wave solution can then be found. However, most nonlinear, dispersive wave equations are non-integrable. While it is still difficult to determine the full DSW structure for non-integrable equations, a general method exists to find its solitary wave and linear dispersive wave edges if the DSW is of "KdV-type," that is it consists of a monotonic modulated periodic wavetrain with solitary waves at one edge and linear dispersive waves at the other [3, 27]. The reason that this can be done is that for a modulationally stable, nonlinear, periodic dispersive wave, its modulation equations are degenerate at these two edges and have a standard structure, which can be determined without detailed knowledge of the full modulation equations [3, 27].

This work deals with a type of non-standard DSW, that for which there is a resonance between the waves of the DSW and linear, diffractive radiation. This resonance has a major effect on the DSW structure as the resonant radiation leaks mass and energy from it. The

standard example equations governing such resonant DSWs are the Kahawara equation [28]

$$\frac{\partial w}{\partial t} + 6w\frac{\partial w}{\partial x} + \mu\frac{\partial^3 w}{\partial x^3} + \frac{\partial^5 w}{\partial x^5} = 0 \tag{1}$$

for $\mu \geq 0$, which is the KdV equation with the next higher order, fifth order, dispersion [29] and the equivalent higher order NLS equation

$$i\frac{\partial u}{\partial t} + \frac{1}{2}\frac{\partial^2 u}{\partial x^2} - |u|^2 u + i\mu\frac{\partial^3 u}{\partial x^3} = 0 \tag{2}$$

with the next higher order, third order, dispersion [30, 31, 32, 33]. The Kahawara equation arises for surface water waves when the effect of surface tension is included and the NLS equation with third order dispersion arises in nonlinear fibre optics, with third order dispersion being one of the higher order effects included for femtosecond pulses [34]. The effect of resonant radiation on the DSW structure will be discussed in detail below, but it is sufficient to state here that if the effect of fifth order dispersion for the Kahawara equation is large enough, $\mu \geq 0$ below a critical value, then the classical KdV DSW structure disappears [29, 35], with a strong resonant wavetrain terminated by a Whitham shock, a modulation shock wave in the modulated wave variables, rather than by a KdV-type DSW [35, 36], as illustrated in Figure 1(d). For DSW bearing nonlinear, dispersive wave equations, the corresponding modulation equations are hyperbolic and so, in theory, possess sharp gas dynamic type shock waves in the wave modulation parameters. When he originally derived modulation theory [1, 23, 24], Whitham speculated on the applicability of these modulation shock solutions, which seem to contradict the slowly varying assumption behind modulation theory. Recent work [36, 37] has shown that these modulation jump conditions are applicable and can be used to derive a wide variety of solutions for nonlinear, dispersive wave equations which have been derived in the past using more involved methods, or not at all. Of interest here, they can be used to derive non-KdV type DSW solutions for which there is resonance with radiation, which have been derived in the past using more ad-hoc methods [29, 35].

This work will derive the full range of solutions for the six DSW types which arise as solutions of the equations governing optical beam propagation in the nonlinear optical medium of a nematic liquid crystal [38, 39, 40]. The equations governing optical beam propagation in a nematic liquid crystal consist of an NLS-type equation for the electric field of the optical beam and an elliptic equation for the nematic response. Previous studies [41, 42] have found that linear radiation can be in resonance with the waves of the DSW if the initial beam has a strong enough intensity discontinuity, with a resonant wavetrain propagating ahead of the main DSW. Again, if the intensity jump is large enough, a DSW as such does not occur, with a resonant wavetrain dominating the solution, as for the Kawahara equation (1) [29]. These previous studies did not give satisfactory agreement with numerical solutions of the nematic equations over the full range of intensity jump strengths. The only good agreement was obtained for the so-called dam break case for which the optical intensity rises from 0 and the solution consists of an expansion wave with no DSW structure [41]. The reason that good agreement between theoretical and numerical solutions was not obtained for the other cases is that the first study [41] assumed that the solution was of KdV DSW-type for all the other five regimes, while the second study [42] assumed that the solution always has a gas dynamic shock structure for all these five regimes. It is found here that these two assumptions do not hold over all solution regimes. The DSW is only of (perturbed) KdV-type for small initial intensity jumps. As the initial optical intensity jump increases, the solution structure

changes to the previously mentioned strong resonant wavetrain terminated by a Whitham shock. This is not the same as the shock structure assumed by [42] as this work assumed that the shock was a non-dispersive shallow water equation type shock. It is found here that this approximation is not satisfactory as the full Whitham shock, including dispersion, has to be used to construct the solution in this regime. In addition to these two limiting cases for small and large initial intensity jumps, the solution for the transition regime between these two limits will be constructed.

In the next section, the six solution regimes for the resonant nematic DSW will be described. The basic method used to derive the five non-trivial nematic DSW structures and understand their stability is Whitham modulation theory for the nematic equations, which is detailed in Section 3. In the subsequent sections, the solutions for the five non-trivial regimes (excluding the known dam break solution) will be derived using this and a combination of perturbed and approximate DSW theory. As the solutions for each regime are developed they are compared with full numerical solutions of the nematic equations. In all cases, excellent comparisons are obtained.

2 Nematic Equations and DSW types

Let us consider the propagation of a linearly polarised beam of coherent light through the nonlinear optical medium of a cell filled with a nematic liquid crystal [39, 40]. The light is assumed to propagate in the direction z down the cell with the beam polarised in the y direction. The x coordinate then completes the coordinate triad. Typical physical cell dimensions are 200μm $\times$ 30μm $\times$ 1mm [39]. Nematic molecules are biaxial [39] with a tensor refractive index. There are then two eigendirections for optical beams, termed the ordinary and extraordinary polarisations [1]. Only the extarordinary polarisation is dispersive and able to support solitary waves [1]. Hence, the optical beam will be assumed to be extraodinarily polarised. An added complication of the nematic medium is that if the nematic molecules are initially aligned with their axis, termed the director, orthogonal to the electric field, the optical Freédericksz threshold exists so that a minimum electric field strength is required to overcome the elastic forces of the nematic medium before the molecules can rotate [38, 39]. To overcome this threshold so that milliwatt power optical beams can rotate the nematic molecules (and so change the refractive index of the medium), an external static electric field is applied to pre-tilt the nematic molecules at an angle θ_0 [43]. Low power optical beams are necessary so that there is minimal heating of the nematic as excessive heating can cause the medium to change phase out of the nematic state. A nematic is typically a focusing medium, so that rotation of the nematic molecules by an optical beam increases the refractive index, leading to self-focusing [39, 40]. However, the formation of a DSW requires the medium to be defocusing [3]. It has been found that the addition of small amounts of azo dye to the nematic changes the medium response, so that the nematic becomes defocusing [44]. The addition of the dye increases scattering losses for the optical beam, but these will be neglected in the present work. With this background and these assumptions, in the paraxial, slowly varying envelope approximation [1], the non-dimensional equations governing the propagation of an optical beam in a defocusing nematic are [39, 40, 44, 45]

$$i\frac{\partial u}{\partial z} + \frac{1}{2}\frac{\partial^2 u}{\partial x^2} - 2\theta u = 0, \tag{3}$$

$$\nu\frac{\partial^2\theta}{\partial x^2} - 2q\theta = -2|u|^2. \tag{4}$$

Here, u is the complex-valued slowly varying envelope of the electric field of the optical beam and θ is the extra optically induced rotation of the director beyond the imposed pre-tilt θ_0. The parameter q is proportional to the square of the imposed pre-tilting electric field and ν is the non-dimensional elasticity of the nematic. The electric field equation (3) is a defocusing NLS-type equation and the director equation (4) is forced by the intensity of the electric field. Note that the nematic equations describe bulk waves, including bulk solitary waves, as z is a spatial coordinate, even though it is "time-like" in the context of the NLS-type equation (3). For typical experimental conditions $\nu = O(100)$ [46, 47, 48, 49]. In this limit the nematic response is termed non-local in the sense that the response of the nematic to the optical forcing extends far beyond the waist of the optical beam [39, 40, 45]. This nonlocal response and large value of ν will play a dominating role in the variety of structures possible for the DSW solution of the nematic equations (3) and (4). We note that in the so-called local limit $\nu \to 0$, the nematic equations (3) and (4) reduce to the defocusing NLS equation, whose DSW solution is known [50]. While the nematic equations are of NLS-type, the nematic DSW more resembles a KdV DSW [41, 42] than an NLS DSW [50] due to the large nonlocality ν.

While the system of equations (3) and (4) has been presented in the context of the nonlinear optics of nematic liquid crystals, they are more general than this. The same system of equations arises in the optics of nonlinear thermal optical media [52, 53], for example lead glasses [51, 54, 55], and certain photorefractive crystals [56]. A similar system of equations also arises in simplified models of fluid turbulence [57] and quantum gravity [58].

To generate a DSW we shall use the step initial condition at $z = 0$

$$u = \begin{cases} u_- e^{iv_- x}, & x < 0 \\ u_+ e^{iv_+ x}, & x > 0 \end{cases}, \qquad \theta = \begin{cases} \frac{u_-^2}{q}, & x < 0 \\ \frac{u_+^2}{q}, & x > 0, \end{cases} \tag{5}$$

which is a jump in the amplitude of the optical field and its wavenumber.

The simplest manner in which to analyse the DSW solution of the nematic equations (3) and (4) is to use the polar coordinate transform (Madelung transformation) [3, 41, 42]

$$u = \sqrt{\rho}e^{i\phi}, \quad v = \phi_x. \tag{6}$$

The nematic equations then become the system

$$\frac{\partial\rho}{\partial z} + \frac{\partial}{\partial x}(\rho v) = 0, \tag{7}$$

$$\frac{\partial v}{\partial z} + v\frac{\partial v}{\partial x} + 2\frac{\partial\theta}{\partial x} - \frac{\partial}{\partial x}\left(\frac{\rho_{xx}}{4\rho} - \frac{\rho_x^2}{8\rho^2}\right) = 0, \tag{8}$$

$$\nu\frac{\partial^2\theta}{\partial x^2} - 2q\theta = -2\rho. \tag{9}$$

The importance of this polar form is that in the non-dispersive limit they reduce to the shallow water equations [1] with ρ playing the role of the fluid depth and v playing the role of the fluid velocity. In addition, in the non-dispersive limit these equations are also those for ideal compressible gas flow [1]. The non-dispersive nematic equations can be set in the

Riemann invariant form

$$v + \frac{2\sqrt{2}}{\sqrt{q}}\sqrt{\rho} = R_+ = \text{constant} \quad \text{on} \quad C_+ : \frac{dx}{dz} = V_+ = v + \frac{\sqrt{2}}{\sqrt{q}}\sqrt{\rho} \tag{10}$$

$$v - \frac{2\sqrt{2}}{\sqrt{q}}\sqrt{\rho} = R_- = \text{constant} \quad \text{on} \quad C_- : \frac{dx}{dz} = V_- = v - \frac{\sqrt{2}}{\sqrt{q}}\sqrt{\rho}, \tag{11}$$

with $\theta = \rho/q$. These non-dispersive equations are an important component of finding DSW solutions as they apply outside the DSW itself and its associated resonant wavetrain, if they exist [3, 41, 42].

Before deriving the solutions for the various DSW regimes, same basic properties of solutions of the nematic equations will be presented. The dispersion relation for linear waves will play a key role in the derivation of the nematic DSW solutions. This is found by linearising about the background states $\bar{\rho}$ in ρ and $\bar{v}$ in v, with

$$\rho = \bar{\rho} + \tilde{\rho}e^{i(kx-\omega z)}, \quad v = \bar{v} + \tilde{v}e^{i(kx-\omega z)}, \quad \theta = \frac{\bar{\rho}}{q} + \tilde{\theta}e^{i(kx-\omega z)}, \tag{12}$$

assuming that $|\tilde{\rho}| \ll \bar{\rho}$, $|\tilde{v}| \ll |\bar{v}|$ and $|\tilde{\theta}| \ll \bar{\rho}/q$. The linear dispersion can then be found as [41, 42]

$$\omega = k\bar{v} + \frac{\sqrt{\bar{\rho}k}}{\sqrt{\nu k^2 + 2q}}\left[\frac{\nu k^2 + 2q}{4\bar{\rho}}k^3 + 4k\right]^{1/2}. \tag{13}$$

A fundamental result of this work is that the DSW for the nematic equations (3) and (4) is itself on long x and z scales, while the resonant wavetrain it sheds are short waves with wavenumber k satisfying $\nu k^2 \gg 1$. In this short wave limit, the dispersion relation (13) becomes

$$\omega = k\bar{v} + \frac{1}{2}k^2 + \ldots \tag{14}$$

Let us first consider the solution of the nematic equations (3) and (4) with the step initial condition (5) for no wavenumber jump, so that $v_- = v_+ = 0$. The solution depends strongly on the height $u_- - u_+$ of the jump, with six distinct DSW types being identified. Figure 1 shows typical examples of these six DSW types. Four of these DSW types are similar to those for the Kawahara equation (1). The two remaining relate to the existence of vacuum cases with $\rho = 0$ at some point. The details of these six DSW types are as follows.

1. Type 1, perturbed dispersive shock wave (PDSW): This nematic DSW type resembles the standard KdV DSW [25, 59], with a monotonic modulated wavetrain consisting of bright solitary waves at the leading edge and linear waves at the trailing edge. There is no resonant wavetrain ahead of the DSW as there is no resonance between the phase velocity of a possible resonant wavetrain, determined by (14), with the DSW [41, 42]. As the nematic equations (3) and (4) are bi-directional, there is also a backwards propagating expansion wave, as for the compressible flow shock tube problem [1], which links the level behind u_- and an intermediate shelf of height $|u| = u_i$ behind the DSW. The DSW takes the place of the shock in the shock tube problem. The solution for this DSW type will be found as a perturbation of the KdV DSW.

2. Type 2, radiating dispersive shock wave (RDSW): When the jump height reaches a critical value [41], which will be discussed in detail in Section 4, resonance can exist

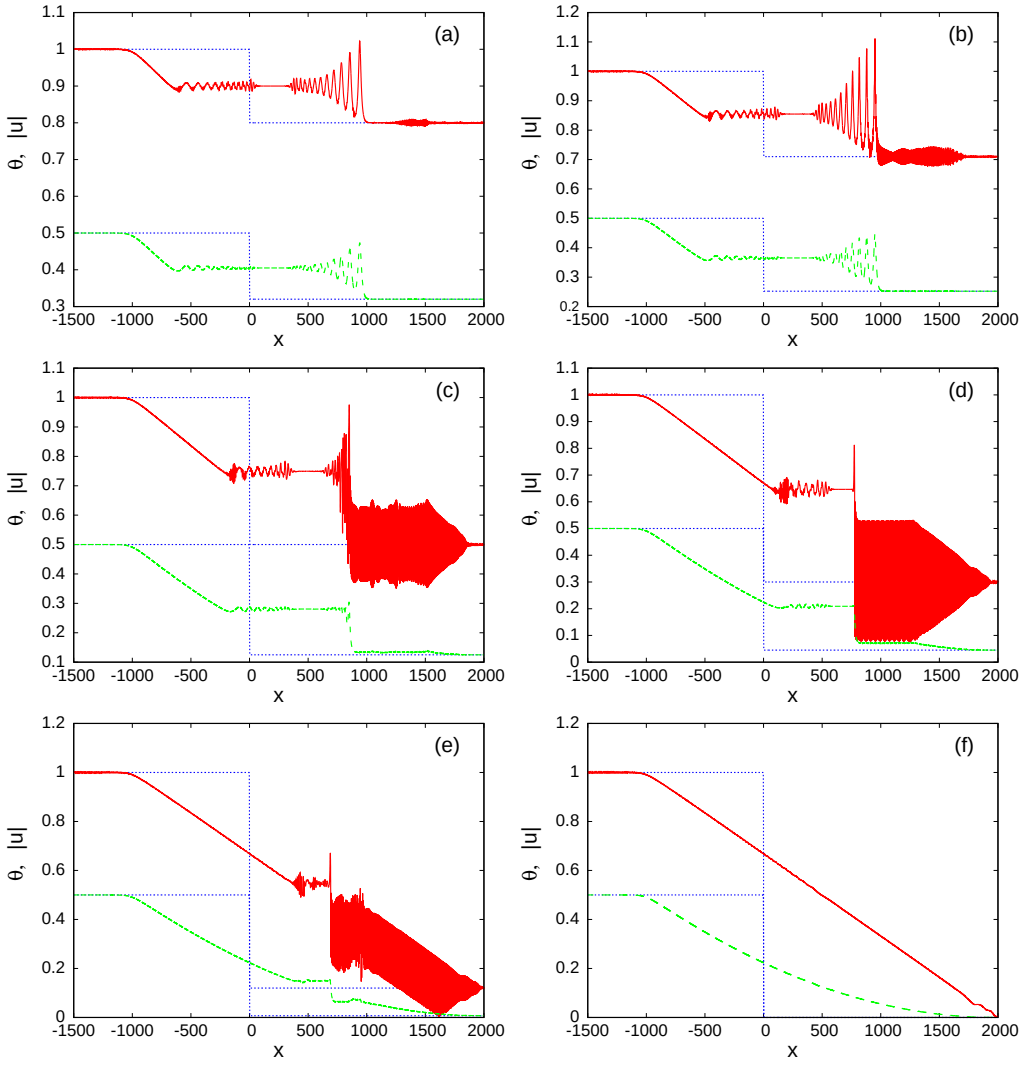


Figure 1: Numerical solutions of nematic equations (3) and (4) for initial condition (5). Red (solid) lines: $|u|$ at $z = 1000$; green (dashed) lines θ at $z = 1000$; blue (dotted) lines: $|u|$ at $z = 0$ (upper) and θ at $z = 0$ (lower). (a) PDSW with $u_+ = 0.8$, (b) RDSW with $u_+ = 0.71$, (c) CDSW with $u_+ = 0.5$, (d) TDSW with $u_+ = 0.3$, (e) VDSW with $u_+ = 0.12$, (f) dam break solution with $u_+ = 0$. Here $u_- = 1$, $\nu = 200$ and $q = 2$.

between the DSW and diffractive waves, so that a resonant wavetrain ahead of the DSW is generated, as shown in Figure 1(b). The DSW itself resembles a KdV DSW, but with an attached resonant wavetrain. This case resembles the equivalent RDSW type for the Kawahara equation (1) [29]. The DSW itself will be found to be a perturbed KdV DSW, as for the PDSW.

3. Type 3, crossover dispersive shock wave (CDSW): With increasing jump height, the DSW becomes unstable, as does its resonant wavetrain, as seen in Figure 1(c). The DSW loses its rank ordered structure and the resonant wavetrain has a highly modulated amplitude. Again, this DSW structure is similar to its equivalent for the Kawahara equation [29].

4. Type 4, travelling dispersive shock wave (TDSW): At a critical jump height, the DSW itself disappears, leaving just a resonant wavetrain, as shown in Figure 1(d). This solution form is similar to the travelling DSW (TDSW) found for the Kawahara equation (1) [29]. A remnant of the DSW is left in the form of a negative polarity solitary wave which links the resonant wavetrain to the intermediate level. It is further seen that the resonant wavetrain is of higher amplitude than in the CDSW case and has stabilised.

5. Type 5, vacuum dispersive shock wave (VDSW): As u_+ decreases, $u_- - u_+$ increases, and the amplitude of the resonant wavetrain grows, the minimum of its oscillation eventually hits the vacuum point $u = 0$, at which point there is a phase singularity and the DSW solution changes form, as seen in Figure 1(e). A constant amplitude resonant wavetrain now propagates on a varying mean level. Behind this, there is a resonant wavetrain on a constant mean level, which is linked to the intermediate level by a negative polarity wave, as for the TDSW. A similar vacuum point solution occurs for the defocusing NLS equation [50], although without the accompanying resonant wavetrain.

6. Type 6 (dam break solution): When the level ahead $u_+ = 0$, the solution becomes essentially non-diffractive, as seen in Figure 1(f). This solution is referred to as the dam break solution as it is the simple wave solution of the shallow water equations (10) and (11) on the characteristic C_- and arises as a solution for the flow generated by a breaking dam [1]. As this dam break solution was considered in detail in previous work [41] and was found to be in near perfect agreement with numerical solutions of the nematic equations (3) and (4), it will not be considered in detail here.

The solution types shown in Figure 1 have the general form that outside the DSW and the resonant wavetrain (if they exist) the solution is non-diffractive and governed by the non-dispersive equations (10) and (11). There is an expansion fan which links the level u_- to an intermediate level u_i, with the DSW (and resonant wavetrain) then taking the solution from $u_i = \sqrt{\rho_i}$ to the level u_+ ahead. The expansion wave is given by the simple wave solution on the characteristic C_- of the Riemann invariant form (10) and (11) of the non-dispersive equations with the Riemann invariant on C_+ constant. If we set the velocity of the trailing edge of the DSW (or Whitham shock, depending on the regime) to be s_i, then this expansion wave solution is [41, 42]

$$|u| = \sqrt{\rho} = \begin{cases} u_-, & \frac{x}{z} < -\frac{\sqrt{2}}{\sqrt{q}}u_- \\ \frac{\sqrt{q}}{3\sqrt{2}}\left[\frac{2\sqrt{2}}{\sqrt{q}}u_- - \frac{x}{z}\right], & -\frac{\sqrt{2}}{\sqrt{q}}u_- \le \frac{x}{z} \le \frac{\sqrt{2}}{\sqrt{q}}\left(2u_- - 3\sqrt{\rho_i}\right) \\ \sqrt{\rho_i}, & \frac{\sqrt{2}}{\sqrt{q}}\left(2u_- - 3\sqrt{\rho_i}\right) < \frac{x}{z} \le s_i, \end{cases} \tag{15}$$

with $v = 2\sqrt{2}(u_- - \sqrt{\rho})/\sqrt{q}$. It is then clear that

$$v = v_i = \frac{2\sqrt{2}}{\sqrt{q}}\,(u_- - \sqrt{\rho_i}) \tag{16}$$

on the intermediate shelf. Previous work has shown that this expansion wave solution is in excellent agreement with full numerical solutions of the nematic equations (3) and (4) [41, 42], so it will not be compared with numerical solutions in this work. To determine the height $u_i = \sqrt{\rho_i}$ of the intermediate shelf and the velocity s_i of its leading edge, the DSW needs to be determined. The dam break problem corresponds to $\rho_i = 0$, in which case $v_i = 2u_-\sqrt{2/q}$ [41].

In the small amplitude limit, the nematic equations (3)–(4) can be reduced to a KdV equation [41, 42, 60] on using the expansions

$$|u| = \sqrt{\rho} = u_0 + \epsilon^2 u_1(\xi,\eta) + \epsilon^4 u_2(\xi,\eta) + \ldots, \tag{17}$$

$$v = \epsilon^2 V_1(\xi,\eta) + \epsilon^4 V_2(\xi,\eta) + \epsilon^6 V_3(\xi,\eta) + \ldots, \tag{18}$$

$$\theta = \frac{u_0^2}{q} + \epsilon^2\theta_1(\xi,\eta) + \epsilon^4\theta_2(\xi,\eta) + \epsilon^6\theta_3(\xi,\eta) + \ldots \tag{19}$$

for small deviations from the level u_0, with $|\epsilon| \ll 1$ being a measure of this deviation. In the moving, scaled coordinates $\xi = \epsilon\,(x - Uz)$ and $\eta = \epsilon^3 z$, with $U^2 = (2/q)u_0^2$, the correction u_1 satisfies a KdV equation with fifth order dispersion, or Kawahara equation, [28, 42]

$$\frac{\partial u_1}{\partial \eta} + 3\sqrt{\frac{2}{q}}u_1\frac{\partial u_1}{\partial \xi} + \sqrt{\frac{2}{q}}\frac{u_0}{4}\left(\frac{\nu}{q} - \frac{q}{4u_0^2}\right)\frac{\partial^3 u_1}{\partial \xi^3} + \sqrt{\frac{2}{q}}\frac{3\epsilon^2\nu^2u_0^2}{16q^2}\frac{\partial^5 u_1}{\partial \xi^5} = 0. \tag{20}$$

Note that in the highly nonlocal limit $\nu \gg 1$ the coefficient of the third derivative term is positive, so that solitary waves are waves of elevation, which explains why the DSWs illustrated in Figure 1 are similar to KdV-type DSWs of elevation with solitary waves at the leading edge and linear diffractive waves at the trailing edge, not NLS-type DSWs, which consist of waves of depression for which the positions of the solitary waves and linear diffractive waves are reversed [50]. The fifth derivative term is nominally of higher order, but due to the high nonlocality ν the combination $\epsilon\nu$ can be $O(1)$ [42]. This reduction of the nematic equations to the Kawahara equation explains the presence of the resonant wavetrains seen in Figure 1 as it has been shown that for the Kawahara equation (1) linear diffractive waves resonate with the DSW if $\mu > 0$. In this case, the Kawahara DSW can be a RDSW, CDSW or TDSW, depending on the value of μ. The vacuum cases of Figures 1(d) and (e) cannot occur for a KdV DSW. They arise for the nematic DSW and NLS-type DSWs due to the requirement $|u| \geq 0$. The Kawahara equation reduction of the full nematic equations will be used in Sections 4–5 to derive the DSW solution as the cases studied there correspond to a small jump height $u_- - u_+$.

The analytical solutions for the DSW in the five regimes, excluding the previously studied dam break limit, will be compared with full numerical solutions of the nematic equations. The nematic equations (3) and (4) were solved numerically using a pseudo-spectral method, with the x derivatives calculated in Fourier space and the solution advanced in z in Fourier space using the fourth order Runge-Kutta scheme. This pseudo-spectral scheme is based on the classic scheme of Fornberg and Whitham [59], but extended to improve its stability and accuracy [61, 62]. The propagation in z using the Runge-Kutta scheme is done in Fourier

space with the dispersion u_{xx} propagated using an integrating factor, which improves stability at high wavenumbers, see [61]. The step initial condition (5) was smoothed using a hyperbolic tangent with a width w. In addition, as a Fourier method is used, periodicity at the ends of the computational domain is ensured by transforming the step into a "top hat." The smoothed initial condition used in the numerical solutions was then

$$u(x,0) = \left[\frac{1}{2}(u_- - u_+)\left(\tanh\frac{x+D}{W} - \tanh\frac{x}{W}\right) + u_+\right] e^{i\phi}, \tag{21}$$

with $v = \phi_x$ smoothed in a similar fashion with u_- replaced by v_- and u_+ replaced by v_+. The width W was chosen to be large enough to stop instabilities, but small enough to well approximate a step. In practice, $W = 1$ was found suitable. The distance D at which the initial condition goes back to the level u_+ was chosen large enough so that the waves generated from the step at $x = 0$ do not interact with the step down, with $D = -10000$ found suitable. Finally, a suitable number of Fourier modes was $N = 131072$, with a z step $dz = 0.002$. All the comparisons with numerical solutions will be for the parameter choices $q = 2$ and $\nu = 200$. In particular, the value of the nonlocality ν depends on the beam power and wavelength, but $\nu = 200$ is typical for near-infrared beams of milliwatt powers [46, 47, 48, 49].

3 Modulation Theory

The key to understanding the behaviours of and for deriving solutions for the nematic DSW and its associated resonant wavetrain will be a solution for the resonant wavetrain and a knowledge of its stability. To study this stability, Whitham modulation theory will be used to generate modulation equations for the periodic wave solution of the nematic equations [1]. Unfortunately, there are no known general solitary wave or periodic wave solutions of the nematic equations. However, the resonant wavetrain has small amplitude, so that the periodic wave solution will be found as a Stokes' expansion, as was done for the Kahawara equation [29] and the fifth order KdV equation, the Kahawara equation (1) with $\mu = 0$ [35]. We then seek a Stokes' expansion solution of the nematic equations as

$$\rho = \bar{\rho} + a\cos\varphi + a^2\rho_2\cos 2\varphi + a^3\rho_3\cos 3\varphi + \ldots, \tag{22}$$

$$v = \bar{v} + av_1\cos\varphi + a^2v_2\cos 2\varphi + a^3v_3\cos 3\varphi + \ldots, \tag{23}$$

$$\theta = \frac{\bar{\rho}}{q} + a\theta_1\cos\varphi + a^2\theta_2\cos 2\varphi + a^3\theta_3\cos 3\varphi + \ldots, \tag{24}$$

$$\omega = \omega_0 + a\omega_1 + a^2\omega_2 + \ldots, \tag{25}$$

where the phase is $\varphi = kx - \omega z$. As is standard, we now substitute the expansions (22)–(25) into the nematic equations (3)–(4) and solve the equations at each order of a, eliminating secular terms by appropriately choosing the ω_j. At $O(a)$ we find the linear dispersion relation

$$\omega_0 = k\bar{v} + \frac{\sqrt{\bar{\rho}}k}{\sqrt{\nu k^2 + 2q}}\left[\frac{\nu k^2 + 2q}{4\bar{\rho}}k^3 + 4k\right]^{1/2}, \tag{26}$$

in accordance with (13). At $O(a^2)$ we find there are no secular terms and

$$\omega_1 = 0, \quad v_1 = \frac{1}{\sqrt{\bar{\rho}\,k\,(\nu\,k^2 + 2\,q)}}\left[4k + \frac{(\nu\,k^2 + 2\,q)\,k^3}{4\bar{\rho}}\right]^{1/2}, \quad \theta_1 = \frac{2}{\nu\,k^2 + 2\,q}. \tag{27}$$

Finally, at $O(a^3)$ to eliminate secular terms we find the nonlinear dispersion relation correction

$$\omega_2 = -\left[\frac{k^4\nu + 2\,k^2 q + 16\,\bar{\rho}}{\nu\,k^2 + 2\,q}\right]^{1/2} \frac{k^6\nu^2 + 5k^4\nu\,q/2 + 12\,k^2\nu\,\bar{\rho} + k^2q^2 + 8\,q\bar{\rho}}{8\bar{\rho}^2 k\,(k^4\nu^2 + 5k^2\nu\,q/2 + q^2 - 4\,\nu\,\bar{\rho})}. \tag{28}$$

The next order terms in the expansions ρ_2, v_2 and θ_2 are not needed and so are not given here.

This Stokes' expansion will be used to calculate the Whitham modulation equations for the Stokes' wave. The expressions for v_1 and ω_2 are involved and not really suitable to calculate amenable modulation equations. Fortunately, the resonant wavetrain is a short wave relative to the DSW and the nonlocal limit of ν large can be taken, as in calculating the short wave linear dispersion relation (14). We also note that this is the physical limit in experiments [46, 47, 48, 49]. Taking this nonlocal limit, we have

$$v_1 = \frac{k}{2\bar{\rho}} + \frac{4}{\nu\,k^3} - \frac{8qk^2 + 16\bar{\rho}}{\nu^2 k^7} + \ldots, \quad \theta_1 = \frac{2}{\nu\,k^2} - \frac{4q}{k^4\nu^2} + \ldots \tag{29}$$

and the dispersion relation amplitude correction

$$\omega_2 = -\frac{k^2}{8\bar{\rho}^2} - \frac{3}{k^2\nu\,\bar{\rho}} - \frac{20\bar{\rho} - 6qk^2}{\nu^2 k^6\bar{\rho}} + \ldots \tag{30}$$

To calculate Whitham modulation equations, either a Lagrangian for the governing equations, or conservation laws for these equations can be used, or a mixture of both [1, 22, 23]. The use of Lagrangians has resulted in this method of analysing slowly varying modulated wavetrains also being termed the method of averaged Lagrangians. As for the determination of the modulation equations for the KdV equation, it was found that a combination of an averaged Lagrangian and conservation equations is optimal [1, 23]. The nematic equations in shallow water form (7)–(9) have the Lagrangian

$$L = -2\rho\phi_z - \frac{1}{4}\frac{\rho_x^2}{\rho} - \rho\phi_x^2 - 4\rho\theta + \nu\theta_x^2 + 2q\theta^2. \tag{31}$$

The nematic equations (7)–(9) also have the "mass" conservation equation

$$\frac{\partial}{\partial z}\rho + \frac{\partial}{\partial x}\rho v = 0, \tag{32}$$

the "momentum" conservation equation

$$\frac{\partial}{\partial z}(\rho v) + \frac{\partial}{\partial x}\left[\rho v^2 - \frac{1}{4}\rho_{xx} + \frac{\rho_x^2}{4\rho} - \frac{1}{2}\nu\theta_x^2 + q\theta^2\right] = 0 \tag{33}$$

and the "energy" conservation equation

$$\frac{\partial}{\partial z}\left[\rho v^2 + \frac{\rho_x^2}{4\rho} + 4\rho\theta - \nu\theta_x^2 - 2q\theta^2\right] + \frac{\partial}{\partial x}\left[\rho v^3 + \frac{1}{2}\rho_x v_x + \frac{3v\rho_x^2}{4\rho} - \frac{1}{2}v\rho_{xx} + 4\rho v\theta + 2\nu\theta_x\theta_z\right] = 0. \tag{34}$$

The mass and momentum conservation equations follow directly from (7)–(9). The easiest method to determine the energy conservation equation is to use Nöther's Theorem on the

Lagrangian (31) based on invariances with respect to z [63]. The terms mass, momentum and energy equations are used in the sense of invariances of the Lagrangian (31) and how they arise in water wave theory. While these terms will be used here, in optics they have different interpretations. For instance, the mass conservation equation (32) is conservation of optical power. Finally, there is the wave conservation equation

$$\frac{\partial k}{\partial z} + \frac{\partial \omega}{\partial x} = 0. \tag{35}$$

This is based on the definition of the slowly varying wavenumber $k = \varphi_x$ and frequency $\omega = -\varphi_z$ in terms of the (slowly varying) phase φ.

The averaged Lagrangian for the Stokes' wave (22)–(24) is calculated by substituting this weakly nonlinear wave into the Lagrangian (31) and averaging by integrating over a period, that is integrating in φ from 0 to 2π. In conjunction with the Madelung transformation (6), a pseudo-phase ψ is introduced for the mean flow $\bar{v}$ with $\gamma = -\psi_z$ and $\bar{v} = \psi_x$, as is standard for Whitham modulation theory, in particular for the modulation equations for the KdV equation [1, 23]. This results in the consistency equation

$$\frac{\partial \bar{v}}{\partial z} + \frac{\partial \gamma}{\partial x} = 0, \tag{36}$$

which is analogous to the wave conservation equation (35). We then have that the averaged Lagrangian is

$$\mathcal{L} = 2\gamma\bar{\rho} - \bar{\rho}\bar{v}^2 - 2\frac{\bar{\rho}^2}{q} + \left[\frac{\omega}{2\bar{\rho}} - \frac{1}{4}\frac{k^2}{\bar{\rho}} - \frac{1}{2}\frac{k\bar{v}}{\bar{\rho}}\right] a^2 + \dots \tag{37}$$

to $O(a^2)$. Note that to obtain the Stokes' expansion dispersion relation (25) by taking variations with respect to a, the averaged Lagrangian is needed to $O(a^4)$. However, this dispersion relation is known via (25), so that averaged wave conservation can be directly calculated by averaging the wave conservation equation (35) using this dispersion relation. So these $O(a^4)$ terms are not needed here.

Taking variations of the averaged Lagrangian (37) with respect to the pseudo-phase ψ

$$\frac{\partial}{\partial z}\frac{\partial \mathcal{L}}{\partial \gamma} - \frac{\partial}{\partial x}\frac{\partial \mathcal{L}}{\partial \bar{v}} = 0 \tag{38}$$

results in the averaged mass conservation equation

$$\frac{\partial \bar{\rho}}{\partial z} + \frac{\partial}{\partial x}\left[\bar{\rho}\bar{v} + \frac{k}{4\bar{\rho}}a^2\right] = 0, \tag{39}$$

which can also be obtained by directly averaging the mass conservation equation (32). Taking variations with respect to the phase φ

$$\frac{\partial}{\partial z}\frac{\partial \mathcal{L}}{\partial \omega} - \frac{\partial}{\partial x}\frac{\partial \mathcal{L}}{\partial k} = 0 \tag{40}$$

gives the conservation of wave action equation

$$\frac{\partial}{\partial z}\frac{a^2}{\bar{\rho}} + \frac{\partial}{\partial x}\left(\frac{\bar{v}}{\bar{\rho}} + \frac{k}{\bar{\rho}}\right) a^2 = 0. \tag{41}$$

Averaging the conservation of waves equation (35) gives

$$\frac{\partial k}{\partial z}+\frac{\partial}{\partial x}\left(k\bar{v}+\frac{1}{2}k^2-\frac{k^2}{8\bar{\rho}^2}a^2+\frac{2\bar{\rho}}{q}\right)=0. \tag{42}$$

Note that to obtain the dispersion relation for the original phase ϕ, rather than for $v=\phi_x$, the mean term $2\bar{\rho}/q$ needs to be added to the v dispersion relation (13) (and (26)) on integration to account for the solution of the nematic equations with $a=0$, that is the constant level solution [41, 42].

To obtain the final modulation equation for the modulation variables $\bar{\rho}$, $\bar{v}$, a and k, it is easiest to average the momentum conservation equation (33) directly. A major reason for this is that this conservation equation will be used in Sections 6 and 7 to determine the DSW and its associated resonant wavetrain in the TDSW and VDSW regimes. This averaged momentum conservation equation is

$$\frac{\partial}{\partial z}\left[\bar{\rho}\bar{v}+\frac{k}{4\bar{\rho}}a^2\right]+\frac{\partial}{\partial x}\left[\bar{\rho}\bar{v}^2+\frac{\bar{\rho}^2}{q}+\left(\frac{\bar{v}k}{2\bar{\rho}}+\frac{k^2}{4\bar{\rho}}\right)a^2\right]=0. \tag{43}$$

Finally, there is the energy conservation equation (34). The averaged energy conservation equation will again be needed in Sections 6 and 7 to determine the DSW solutions in the TDSW and VDSW regimes. This is because shock jump conditions for the Whitham modulation equations will be used to determine the resonant wavetrain [1, 36] and these are derived from averaged conservation equations [1]. The averaged energy conservation equation is

$$\frac{\partial}{\partial z}\left[\bar{\rho}\bar{v}^2+\frac{2}{q}\bar{\rho}^2+\left(\frac{k\bar{v}}{2\bar{\rho}}+\frac{k^2}{4\bar{\rho}}\right)a^2\right]+\frac{\partial}{\partial x}\left[\bar{\rho}\bar{v}^3+\frac{4}{q}\bar{\rho}^2\bar{v}+\left(\frac{3\bar{v}^2k}{4\bar{\rho}}+\frac{3\bar{v}k^2}{4\bar{\rho}}+\frac{k^3}{4\bar{\rho}}+\frac{k}{q}\right)a^2\right]=0. \tag{44}$$

The Whitham modulation equations (39), (41), (42) and (43) will be used to derive solutions for the resonant wavetrain and to determine the modulational stability of this wavetrain. For this purpose, they need to ideally be set in Riemann invariant form if they form a hyperbolic system. After extensive algebra, they can be set in the Riemann variable form [1]

$$-\frac{32\lambda_1\bar{\rho}^2a}{k\left(qk^2-10\bar{\rho}\right)}\frac{d\bar{\rho}}{dz}-\frac{8\lambda_1\bar{\rho}^2\left(qk^2-2\bar{\rho}\right)a}{k^2\left(qk^2-10\bar{\rho}\right)}\frac{dk}{dz}+\frac{da^2}{dz}-\frac{8\lambda_1\bar{\rho}^2\left(qk^2+2\bar{\rho}\right)a}{k^2\left(qk^2-10\bar{\rho}\right)}\frac{d\bar{v}}{dz}=0$$

$$\text{on}\quad \frac{dx}{dz}=\lambda_1=\bar{v}+k+\frac{ka}{4\bar{\rho}}\sqrt{\frac{20\,\bar{\rho}-2k^2q}{qk^2-2\,\bar{\rho}}}, \tag{45}$$

$$\frac{32\lambda_1\bar{\rho}^2a}{k\left(qk^2-10\bar{\rho}\right)}\frac{d\bar{\rho}}{dz}+\frac{8\lambda_1\bar{\rho}^2\left(qk^2-2\bar{\rho}\right)a}{k^2\left(qk^2-10\bar{\rho}\right)}\frac{dk}{dz}+\frac{da^2}{dz}+\frac{8\lambda_1\bar{\rho}^2\left(qk^2+2\bar{\rho}\right)a}{k^2\left(qk^2-10\bar{\rho}\right)}\frac{d\bar{v}}{dz}=0$$

$$\text{on}\quad \frac{dx}{dz}=\lambda_2=\bar{v}+k-\frac{ka}{4\bar{\rho}}\sqrt{\frac{20\,\bar{\rho}-2k^2q}{qk^2-2\,\bar{\rho}}}, \tag{46}$$

$$\sqrt{\frac{2}{q}}\frac{1}{\sqrt{\bar{\rho}}}\frac{d\bar{\rho}}{dz}+\frac{a^2}{4\bar{\rho}^2+2qk^2\bar{\rho}-4\sqrt{2q}k\bar{\rho}^{3/2}}\frac{dk}{dz}+\frac{\sqrt{2q}k}{4\bar{\rho}^{3/2}\left(\sqrt{2q}\sqrt{\bar{\rho}}-qk\right)}\frac{da^2}{dz}+\frac{d\bar{v}}{dz}=0$$

$$\text{on}\quad \frac{dx}{dz}=\lambda_3=\bar{v}+\sqrt{\frac{2}{q}}\sqrt{\bar{\rho}}+\frac{ka^2}{2\bar{\rho}}\frac{2\sqrt{2\bar{\rho}}-\sqrt{q}k}{\sqrt{2\bar{\rho}}\left(qk^2+2\,\bar{\rho}\right)-4\sqrt{q}\,k\bar{\rho}}, \tag{47}$$

$$-\sqrt{\frac{2}{q}}\frac{1}{\sqrt{\bar{\rho}}}\frac{d\bar{\rho}}{dz}+\frac{a^2}{4\bar{\rho}^2+2qk^2\bar{\rho}+4\sqrt{2q}k\bar{\rho}^{3/2}}\frac{dk}{dz}+\frac{\sqrt{2q}k}{4\bar{\rho}^{3/2}\left(\sqrt{2q}\sqrt{\bar{\rho}}+qk\right)}\frac{da^2}{dz}+\frac{d\bar{v}}{dz}=0$$

$$\text{on} \quad \frac{dx}{dz} = \lambda_4 = \bar{v} - \sqrt{\frac{2}{q}}\sqrt{\bar{\rho}} + \frac{ka^2}{2\bar{\rho}} \frac{2\sqrt{2\bar{\rho}} + \sqrt{q}k}{\sqrt{2\bar{\rho}}\,(qk^2 + 2\,\bar{\rho}) + 4\sqrt{q}\,k\bar{\rho}} \tag{48}$$

to $O(a^2)$. Note that at the leading order with $a = 0$, the two characteristic forms (47) and (48) are the shallow water equations in Riemann variable form [1], which must be the case. The system (45)–(48) is hyperbolic if the wavenumber k falls within the restricted range

$$\bar{u} < \sqrt{\frac{q}{2}}\,k < \sqrt{5}\,\bar{u}, \tag{49}$$

as $\bar{u} = \sqrt{\bar{\rho}}$. The Stokes wavetrain is then modulationally stable for k in the range (49) and unstable otherwise. The restricted range of the wavenumber for stability leads to the resonant wavetrain generated by the DSW to be unstable over a great portion of the range of its existence. Unfortunately, it was not found possible to set the Riemann variable form (45)–(48) into Riemann invariant form, a manifestation of Pfaff's problem. Outside the range (49) the system (45)–(48) is mixed elliptic-hyperbolic since the characteristics (47) and (48), which are those for the shallow water equations at leading order, are always real. This is important as in Sections 6 and 7 the Riemann variables on these characteristics are be used to construct the solutions in the TDSW and VDSW regimes.

In the next sections the solutions for the five non-trivial nematic DSW regimes, the PDSW, RDSW, CDSW, TDSW and VDSW will be found and compared with numerical solutions of the nematic equations (3) and (4). Different analytical methods will be used to derive the DSW solutions in these five regimes. Comparisons of DSW parameters with numerical solutions will be made separately as the solution in each regime is found, even though the DSW parameters, such as resonant wave height and resonant wavenumber, are common across some, or all, of the regimes and there is no solution distinction in the numerical parameters.

4 Perturbed Nematic DSW and RDSW

In this section, the solution for the perturbed DSW (PDSW), illustrated in Figure 1(a), and the radiating DSW, illustrated in Figure 1(b), will be found based on the Kawahara equation reduction (20) of the full nematic equations as these DSW solutions are valid for small jump heights $u_i - u_+$. The DSWs in these two regimes are similar to the KdV DSW, with solitary waves at the leading edge and linear diffractive waves at the trailing edge. While the DSW radiates resonant waves in the RDSW regime, the effect of this loss is small and can be neglected to find the DSW solution. The resonant radiation loss becomes dominate in the CDSW regime.

It was shown that the KdV equation with all the next higher order nonlinear, dispersive and nonlinear-dispersive terms of relative order α in the weakly nonlinear, long wave expansion used to derive the KdV equation [1]

$$\frac{\partial \eta}{\partial T} + 6\eta\frac{\partial \eta}{\partial X} + \alpha C_1\eta^2\frac{\partial \eta}{\partial X} + \frac{\partial^3 \eta}{\partial X^3} + \alpha C_2\frac{\partial \eta}{\partial X}\frac{\partial^2 \eta}{\partial X^2} + \alpha C_3\eta\frac{\partial^3 \eta}{\partial X^3} + \alpha C_4\frac{\partial^5 \eta}{\partial X^5} = 0 \tag{50}$$

can be transformed to the KdV equation ((1) with $\mu = 1$ and no fifth derivative term) with error $O(\alpha^2)$ [64], which is of higher order than the validity of the original equation. This transformation was then used to find the DSW solution of the higher order KdV equation (50) from that for the KdV equation [64]. This perturbed DSW solution will be used to

find the perturbed DSW solution of the reduction (20) of the nematic equations. The KdV reduction (20) of the nematic equations does not contain the higher order terms $u_1^2 u_{1\xi}$, $u_{1\xi} u_{1\xi\xi}$ and $u_1 u_{1\xi\xi\xi}$ of the general higher order KdV equation (50). The reason for this can most easily be seen on expanding the nematic dispersion relation (13) in the long wave limit $k \ll 1$, giving

$$\omega = k\left(\sqrt{\frac{2}{q}}\bar{u} + \bar{v}\right) - \frac{c}{4}\left(\frac{\nu}{q} - \frac{q}{4\bar{\rho}}\right)k^3 + \frac{c}{32}\left(\frac{3\nu^2}{q^2} + \frac{\nu}{\bar{\rho}} - \frac{q^2}{16\bar{\rho}^2}\right)k^5 + \ldots, \tag{51}$$

with $\bar{u} = \sqrt{\bar{\rho}}$. We note that this dispersion relation does not contain a term $\bar{u}^2 k$, so that there is no higher order nonlinear term $u_1^2 u_{1\xi}$. In addition, the fifth derivative term in (50) was obtained by including the fifth derivative from higher order in the expansion (17)–(19) as the coefficient $\epsilon^2\nu^2$ can be $O(1)$ as ν is large. In a similar manner, the higher order nonlinear/dispersive terms $u_{1\xi} u_{1\xi\xi}$ and $u_1 u_{1\xi\xi\xi}$ would be at most $O(\epsilon^2\nu)$ and so can be ignored.

The transformation of [64] then gives that the PDSW is a modulated, perturbed cnoidal wave of amplitude a (measured peak to trough), wavenumber k and mean height $\bar{u}$. On identifying $u_0 = u_+$ and $\epsilon^2 = u_i - u_+$ in the perturbation expansions (17)–(19), we have from [64] that the PDSW solution is given by

$$a = 2(u_i - u_+)m + 2C_4(u_i - u_+)^2 m\left(\frac{8}{3} - m\right), \tag{52}$$

$$k = \frac{\pi\sqrt{2(u_i - u_+)}}{K(m)\sqrt{u_+}\sqrt{\frac{\nu}{q} - \frac{q}{4u_+^2}}}\left[1 - \frac{1}{3}C_4\left(8m^2 - 14m + 11\right)(u_i - u_+)\right], \tag{53}$$

$$\begin{aligned}\bar{u} = {} & 2u_+ - u_i + (u_i - u_+)\left(2\frac{E(m)}{K(m)} + m\right) \\ & + \frac{2}{9}C_4(u_i - u_+)^2\left[2 - 5m + 3m^2 + 2(2m-1)\frac{E(m)}{K(m)}\right] \\ & + \frac{32}{9}C_4(u_i - u_+)^2\left[3\left(1 - \frac{E(m)}{K(m)}\right)^2 - 2\left(1 - \frac{E(m)}{K(m)}\right)(1+m) + m\right]\end{aligned} \tag{54}$$

on

$$\begin{aligned}\frac{x}{z} = {} & \sqrt{\frac{2}{q}}\left[u_+ + \frac{1}{2}\lambda - \frac{1}{3}C_4\lambda_1 + \frac{1}{6}C_4\lambda^2 - \frac{4}{3}C_4(u_i - u_+)^2[m(2-m) - 1]\right. \\ & \left. - \frac{4}{3}C_4(u_i - u_+)\left(m - 1 + \frac{2E(m)}{K(m)}\right)(\lambda - V)\right],\end{aligned} \tag{55}$$

with

$$V = 2(u_i - u_+)(1+m) - \frac{4}{3}C_4(u_i - u_+)^2(3m - 3m^2 - 2), \tag{56}$$

and

$$\lambda = V - \frac{4(u_i - u_+)m(1-m)K(m)}{E(m) - (1-m)K(m)}, \quad \lambda_1 = 2(u_i - u_+)^2\left[1 + m - \frac{2m(1-m)K(m)}{E(m) - (1-m)K(m)}\right]. \tag{57}$$

Note that various typographical errors in the asymptotic expressions of [64] have been corrected to obtain the expressions (52)–(57). The coefficient C_4, which comes from rescaling the fifth order KdV equation (1) to the higher order KdV equation (50), is

$$C_4 = \frac{3\nu^2}{2q^2}\left[\frac{\nu}{q} - \frac{q}{4u_+^2}\right]^{-2}. \tag{58}$$

DSW type	numerical existence interval	theoretical existence interval
PDSW	$0.76 < u_+ < 1.0$	$0.73 < u_+ < 1.0$
RDSW	$0.70 < u_+ < 0.76$	$0.70 < u_+ < 0.73$
CDSW	$0.44 < u_+ < 0.70$	$0.44 < u_+ < 0.70$
TDSW	$0.22 < u_+ < 0.44$	$0.24 < u_+ < 0.44$
VDSW	$0 < u_+ < 0.22$	$0 < u_+ < 0.24$
Dam break	$u_+ = 0$	$u_+ = 0$

Table 1: Comparisons between numerical and theoretical existence regions for the six nematic bore types described in Section 2. Here $u_- = 1.0$, $\nu = 200$ and $q = 2$.

Here, $K(m)$ and $E(m)$ are complete elliptic integrals of the first and second kinds of modulus m, respectively. The limit $m = 0$ corresponds to the trailing linear, diffractive wave edge of the PDSW and $m = 1$ corresponds to the leading, solitary wave edge. The DSW then lies within the region

$$s_i = \sqrt{\frac{2}{q}}\left[4u_+ - 3u_i + \frac{64}{3}C_4(u_i - u_+)^2\right] \leq \frac{x}{z} \leq s_+ = \sqrt{\frac{2}{q}}\left[2u_i - u_+ + \frac{4}{3}C_4(u_i - u_+)^2\right]. \tag{59}$$

The amplitude a_s of the solitary wave at the leading edge of the DSW can be found from the amplitude expression (52) on setting $m = 1$. This gives

$$a_s = 2\,(u_i - u_+) + \frac{10}{3}C_4\,(u_i - u_+)^2\,, \tag{60}$$

so that the height H_s of the lead solitary wave of the DSW from $u = 0$ is

$$H_s = a_s + u_+ = 2u_i - u_+ + \frac{10}{3}C_4\,(u_i - u_+)^2\,. \tag{61}$$

The Riemann invariant R_- on the characteristic C_- given by (11) of the non-dispersive equations is conserved through the DSW [3, 27]. As $\rho = u_+^2$ and $v = 0$ at the leading edge of the DSW, $R_- = -2\sqrt{2}u_+/\sqrt{q} = v_i - 2\sqrt{2}u_i/\sqrt{q}$, so that on using expression (16) from the expansion wave solution we have [41, 42].

$$u_i = \frac{1}{2}\,(u_- + u_+)\,, \quad v_i = \frac{\sqrt{2}}{\sqrt{q}}\,(u_- - u_+)\,. \tag{62}$$

This completes the solution for the PDSW.

As previously found [41, 42], a resonance between diffractive radiation and the DSW can occur when the phase velocity of the diffractive radiation equals the velocity s_+ of the lead solitary wave of the DSW. As can be seen from Figure 1(b) this resonant radiation is short wave relative to the DSW, so that the appropriate linear dispersion relation is (14). Resonance then occurs for the wavenumber k_r, with

$$k_r = s_+ + \left(s_+^2 - \frac{4}{q}u_+^2\right)^{1/2}, \tag{63}$$

on taking $v_+ = 0$, which is assuming that the resonant wavetrain sits on the initial level u_+ ahead. If $s_+ \leq 2u_+/\sqrt{q}$, then there is no resonant wavetrain ahead of the DSW, which is the

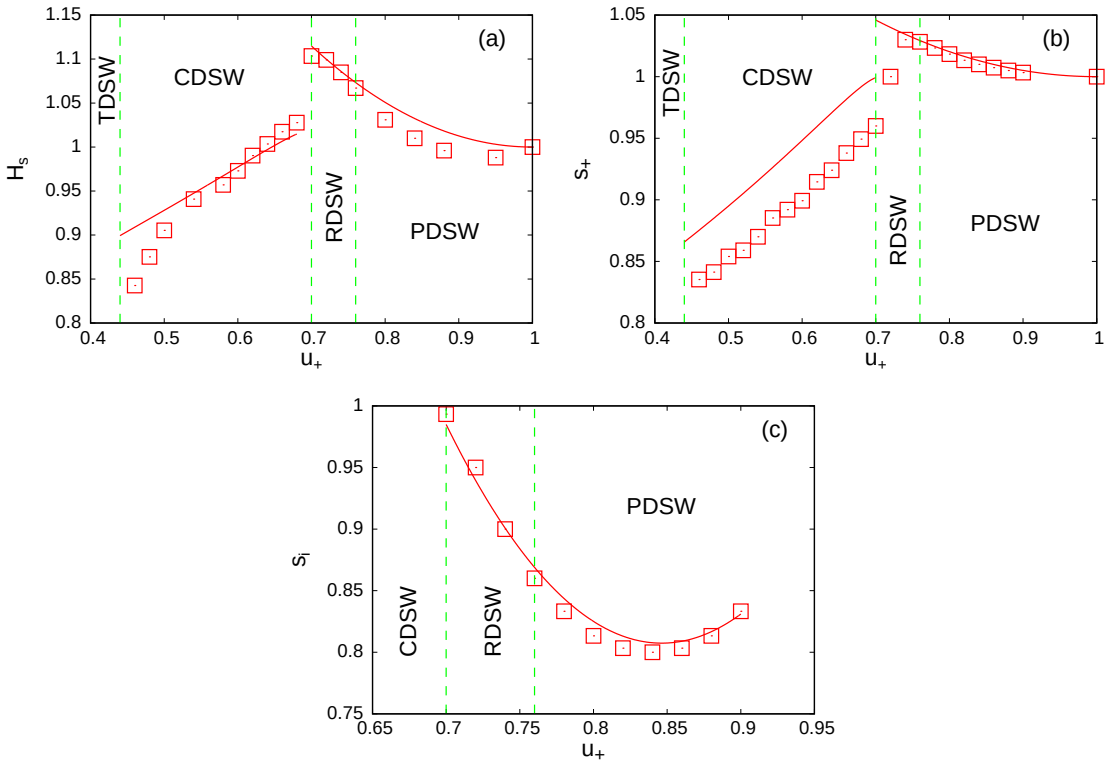


Figure 2: Comparisons between numerical solutions of the nematic equations (3) and (4) and the DSW solutions for the PDSW, RDSW and CDSW regimes. Numerical solution: red boxes; analytical solution: red (solid) line. (a) lead solitary wave height H_s (61), (b) velocity s_+ of leading edge of DSW, (c) velocity s_i of trailing edge of DSW. Here $u_- = 1.0$, $\nu = 200$ and $q = 2$.

PDSW regime illustrated in Figure 1(a). If $s_+ > 2u_+/\sqrt{q}$, then the DSW sheds a resonant wavetrain ahead of it as the group velocity $c_g = k_r$ of the resonant wavetrain is greater than its phase velocity, $c < c_g$ [41, 42], on using (59) and (14). Resonance can then occur if $s_+ \geq 2u_+/\sqrt{q}$. If this condition is not satisfied, then there is just a DSW and we have the PDSW regime.

When the resonance condition (63) has a solution, we have the RDSW regime for the nematic bore, as illustrated in Figure 1(b). It was found that the RDSW regime is also well described by the perturbed KdV DSW solution (52)–(55). This is because the resonant radiation shed by the DSW is of small amplitude, as can be seen from Figure 1(b), and the existence regime for this type is small, as seen from Table 1. The resonant wavetrain has a major effect in the CDSW regime, which is dealt with in the next section, as the resonant wavetrain acts as a damping on the DSW and the DSW is unstable in this regime.

Figure 2 shows comparisons between numerical solutions and the perturbed KdV DSW solution (52)–(55) for the height $H_s = u_+ + a_s$ and velocity s_+ of the lead solitary wave and the velocity s_i of the trailing edge of the DSW. It can be seen that there is excellent agreement for the lead solitary wave height over both the PDSW and RDSW regimes. When a resonant wavetrain is present, the amplitude of the lead wave of the DSW oscillates as radiation propagates out of the DSW [35]. In this case, the average lead wave amplitude is

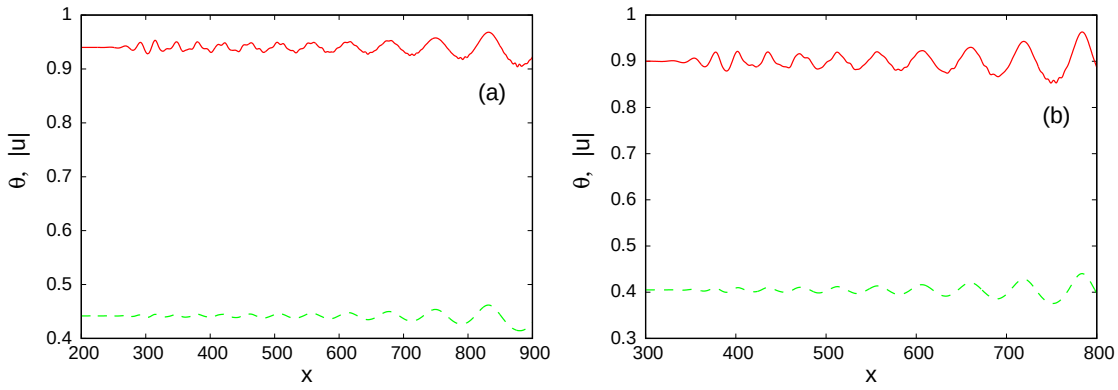


Figure 3: Numerical solutions of the nematic equations (3) and (4) for the initial condition (5) with $u_- = 1$. Red (solid) lines: $|u|$ at $z = 1000$; green (dashed) lines θ at $z = 1000$. (a) PDSW with $u_+ = 0.88$, (b) RDSW with $u_+ = 0.8$. Here $u_- = 1.0$, $\nu = 200$ and $q = 2$.

taken for the numerical comparisons. Figure 2(b) shows that there is also excellent agreement for the velocity s_+ of the leading edge. There is some disagreement in the lead wave height and velocity at the transition from the RDSW to the CDSW regime, but this is to be expected as the DSW drastically changes form. The leading edge velocity does not show much variation from u_- in these PDSW and RDSW regimes. Setting $C_4 = 0$ in the perturbed KdV DSW solution (52)–(55) gives the standard KdV DSW solution, for which $H_s = u_-$ and $s_+ = u_-$ on using (62) for u_i, as found in a previous study [41]. It is then seen that the higher order dispersion in the Kawahara equation (20) is necessary to fully account for the lead solitary wave in the PDSW and RDSW regimes, although the additional effect is not large. Figure 2(c) shows a comparison between numerical solutions and the perturbed KdV DSW solution for the trailing edge velocity s_i. The comparison is again very good, in particular for the turning point in the trailing edge velocity. The implications of this turning point will be discussed below.

The wavenumber of the resonant wavetrain in the RDSW regime is given by the resonance condition (63), which has a solution if $s_+ \geq 2u_+/\sqrt{q}$. Table 1 gives comparisons between the existence intervals for the six DSW regimes as given by numerical solutions and by the analytical solutions for the parameter choices $u_- = 1$, $\nu = 200$ and $q = 2$. In particular, it can be seen that there is good agreement for the intervals of existence for the PDSW solution, which does not have an associated resonant wavetrain as $s_+ < 2u_+/\sqrt{q}$. There is excellent agreement for the existence region of the RDSW, which has an associated resonant wavetrain. Note that the lower bound for the RDSW regime is connected with the existence of the CDSW regime, which is dealt with in Section 5.

At this point the admissibility conditions for the existence of a DSW need to be checked [3, 13]. These relate to the genuine nonlinearity and hyperbolicity of the associated Whitham modulation equations upon which DSW solutions are ultimately based. The breakdown of these lead to linear degeneracy in the first case and modulational instability in the second case, so that the standard DSW solution, as derived above, breaks down. The admissibility conditions require that the derivatives of the velocities of the trailing edge s_i and of the leading edge s_+ do not have turning points as functions of (u_-,u_+). It is found from the leading edge velocity expression (59) for s_+ that these derivatives do not vanish at the leading edge, so there is no breakdown of the DSW structure at the leading edge. At the trailing edge, the derivative

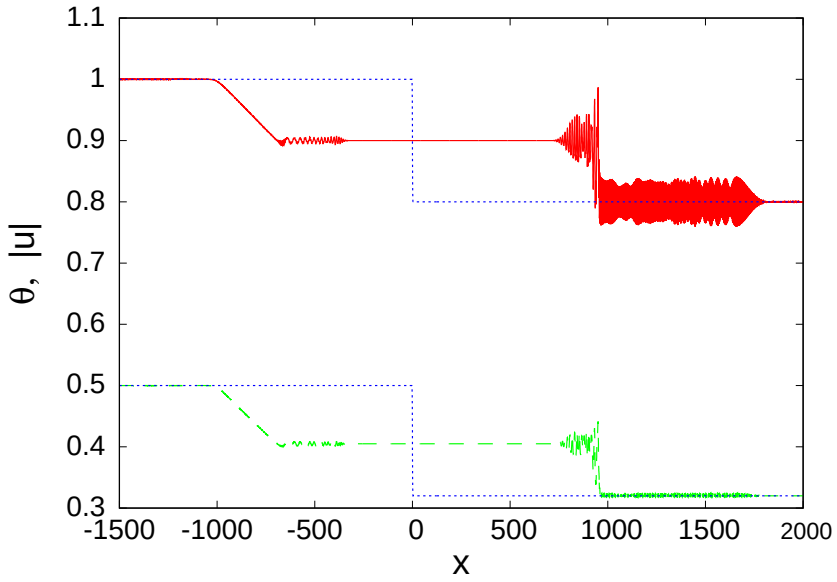


Figure 4: Numerical solution of the nematic equations (3) and (4) for the initial condition (5). Red (solid) line: $|u|$ at $z = 1000$; green (dashed) line θ at $z = 1000$; blue (dotted) lines: $|u|$ at $z = 0$ (upper) and θ at $z = 0$ (lower). Here $u_- = 1.0$, $u_+ = 0.8$, $\nu = 10$ and $q = 2$.

of s_i with respect to u_- vanishes when $u_+ = u_- - 3/32$, which is $u_+ = 0.90625$ for $u_- = 1$, and the derivative with respect to u_+ vanishes when $u_+ = u_- - 5/32$, which is $u_+ = 0.84375$ for $u_- = 1$. In these calculations, C_4 given by (58) has been approximated by $C_4 = 3/2$ as ν is large. The turning point with respect to u_- means that after this point a simple wave solution of the Whitham modulation equations governing the DSW is not possible, while the vanishing of the derivative with respect to u_+ means that the Whitham modulation equations lose hyperbolicity, so that the modulated wavetrain is not stable. The breakdown of these admissibility conditions is usually clearly mirrored in numerical solutions by non-standard DSW behaviour, such as the generation of a multi-phase wavetrain or wavetrain instability [13]. However, for the nematic DSW there is no clear evidence of such behaviour for values of u_+ below the turning points, as seen in Figures 1(a) and (b). These figures show some evidence of instability at the trailing edge of the DSW, but it is minor.

Figure 3 shows details of the trailing edges of DSWs on either side of the predicted onset of modulational instability at $u_+ = 0.84375$. It can be seen that there is some non-uniform modulation of the trailing edges, with a modulated wavepacket, but there is no distinct change in the behaviour of the DSW, as found for other DSWs for which the admissibility conditions are not satisfied [3, 13]. The reason for this is the highly nonlocal response of the nematic. It has been shown theoretically and verified experimentally that high nonlocality acts to suppress modulational instability [65, 66]. This greatly delays the onset of instability, so much so that theoretically unstable nematic wavetrains show no instability over experimental propagation distances ($\sim 1mm$).

The stability of the Stokes' wave solution of the Kawahara equation (1) has been studied [35]. This work can be used to determine the stability of the trailing edge of the DSW, where the wavenumber is k_i given by (53) with $m = 0$. Rescaling the nematic KdV equation (20) to the standard form (1) of the Kawahara equation gives the scaled wavenumber $\tilde{k}_i$ at the

trailing edge of the DSW as

$$\tilde{k}_i = 2\left[1 - \frac{11}{6}C_4\left(u_- - u_+\right)\right]. \tag{64}$$

The work of [35] then gives that the trailing edge of the DSW is stable if

$$15\tilde{k}_i^2\left[\frac{6}{5\tilde{k}_i^2 - 3/C_4} + \frac{1}{5\tilde{k}_i^2 - 1/C_4}\right] + 9 > 0. \tag{65}$$

For the parameter values $\nu = 200$ and $q = 2$, this stability condition gives that the trailing edge of the DSW is unstable for $0.7223 \leq u_+ \leq 0.7547$ and $0.6938 \leq u_+ < 0.7080$. The onset of instability corresponds to the transition from the PDSW to the RDSW regime, as seen from Table 1, and the onset of the generation of resonant radiation. Again, numerical solutions show no evidence of any major instability in this region. The suppression of modulational instability due to the high nonlocality [65, 66] is again presumed to be the reason. This conjecture about the stabilising role of nonlocality is verified by the solution shown in Figure 4, which is for the same initial condition and parameter values as Figure 1(a), except that the nonlocality has been lowered to $\nu = 10$ from $\nu = 200$. The PDSW of Figure 1(a) is stable, but Figure 4 shows that lowering the nonlocality results in a dramatic change in the DSW. It is now unstable, in accord with the admissibility conditions and the modulational instability condition of [35]. In addition, there is now a resonant wavetrain. The resonant condition (63) is valid in the limit $\nu \gg 1$, so is not strictly applicable for $\nu = 10$. Further decrease of the nonlocality ν is not possible as then the coefficient of the third derivative in the nematic Kawahara equation (20) becomes negative and the DSW changes from a positive polarity KdV-type to a negative polarity NLS-type DSW consisting of dark, rather than bright, waves.

The nematic DSW structure instability is driven by the instability of the resonant wavetrain. The Whitham modulation equations (45)–(48) for the resonant wavetrain become elliptic, so that Benjamin-Feir instability arises and the underlying Stokes' wave solution for the resonant wavetrain becomes unstable. The Whitham modulation equations for the nematic Stokes' wave are hyperbolic for wavenumbers in the range (49), so that the weakly nonlinear Stokes' wavetrain is stable in this region. Using the resonance condition (63) with $k = k_r$, s_+ given by (59) and $\bar{u} = u_+$ with $q = 2$ and $\nu = 200$, this gives that the resonant wavetrain is unstable if $u_+ < 0.674$, which from Table 1 is the CDSW regime. However, numerical solutions show that the resonant wavetrain in the RDSW regime is unstable, see Figure 1(b), for instance. The reason for this disagreement between theory and numerical solutions will be discussed in detail in Sections 5–7. It is sufficient to note at this stage that when the resonant wavetrain is unstable, the resonance condition (63) gives a poor prediction of the resonant wavenumber as the wavetrain ceases to be a uniform wavetrain with a single wavenumber, but gives a good prediction when the resonant wavetrain is stable, see Figure 8(c).

Figure 5 shows this modulational instability of the resonant wavetrain for $u_+ = 0.65$. The instability of the resonant wavetrain is now clear, in contrast to the example shown in Figure 1(b), with the breakup of the resonant wavetrain as it propagates in z now prominent. Each wave of the DSW generates a resonant wave as a DSW is a modulated wavetrain [35]. Figure 5 shows that these resonant waves within the DSW are also unstable. Figure 6 further details the evolution of the instability of the resonant wavetrain and shows a transition from a

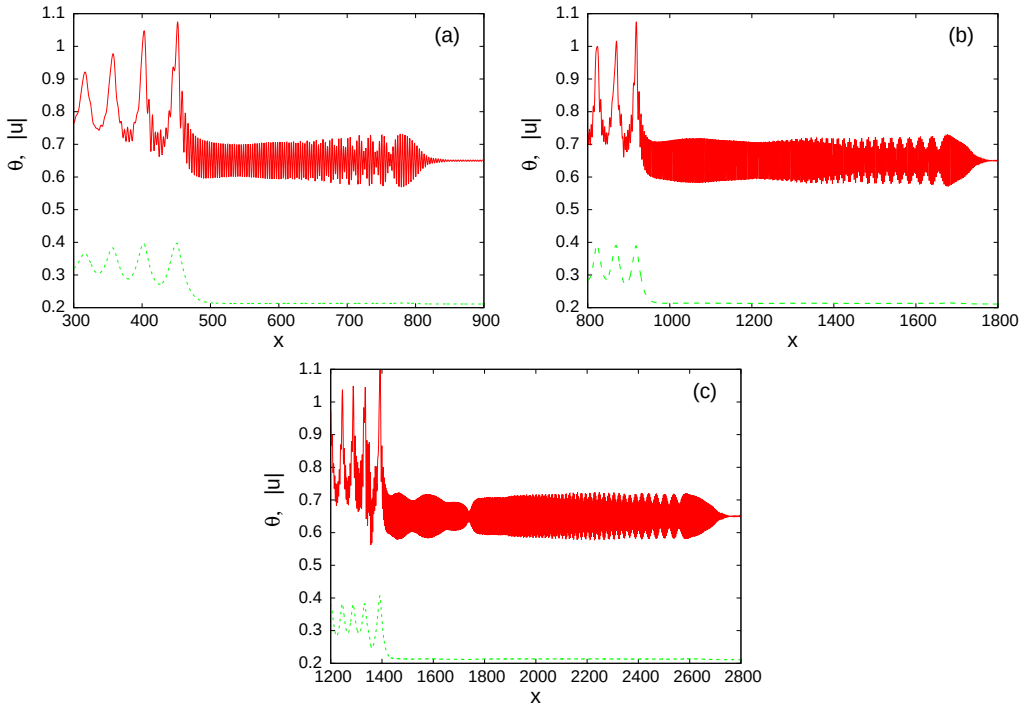


Figure 5: Numerical solutions of the nematic equations (3) and (4). Red (solid) lines: $|u|$; green (dashed) lines: θ. Solutions at (a) $z = 500$, (b) $z = 1000$, (c) $z = 1500$. Here $u_- = 1.0$, $u_+ = 0.65$, $q = 2$ and $\nu = 200$.

uniform wavetrain to a series of wavepackets. This detailed modulational instability evolution closely resembles experimental photographs of Benjamin-Feir instability for water waves [67].

The Stokes' wave expansion (22)–(25) and the associated Whitham modulation equations (45)–(48) are weakly nonlinear and hold for relatively small amplitudes. As the amplitude of the resonant wavetrain rises, it is found numerically that it restabilises, as illustrated in Figure 7, which is an expanded view of the DSW of Figure 1(c). It can be seen that while the resonant wavetrain is not uniform, as for the fifth order KdV resonant wavetrain [35], the degree of modulation is much reduced over that of Figure 5. This resonant wavetrain modulational instability is significant in the CDSW regime, which is analysed in the next section.

5 Nematic Crossover DSW

The solution for the crossover DSW (CDSW) illustrated in Figure 1(c) will now be derived. As can be seen from Figure 1(c), moving to the CDSW regime results in the KdV-type DSW in the PDSW and RDSW regimes becoming unstable, with the waves in the DSW ceasing to have a near linear amplitude decrease, as seen in Figure 7, which gives a detail view of the DSW of Figure 1(c). The numerical leading edge velocity s_+ of Figure 2(b) shows that it has a maximum in u_+ around the boundary between the RDSW and CDSW regimes, so that the admissibility conditions discussed above give that the DSW becomes unstable, matching the numerical behaviour. Figure 1(c) shows that for a large part of the CDSW, the waves have nearly equal amplitudes, with a rapid drop near its trailing edge. As discussed, this

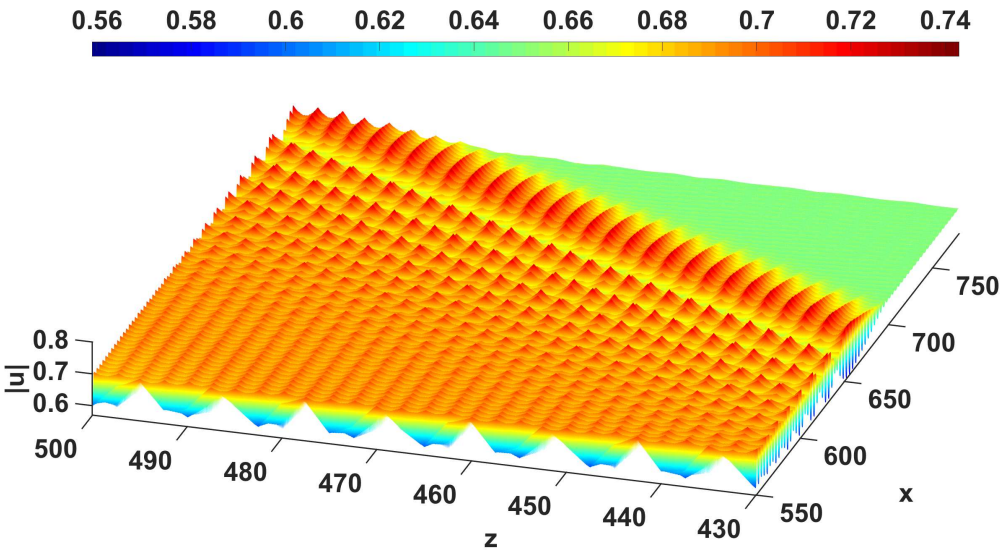


Figure 6: Numerical solution of the nematic equations (3) and (4) for $|u|$ showing evolution of resonant wavetrain instability. Here $u_- = 1.0$, $u_+ = 0.65$, $\nu = 200$ and $q = 2$.

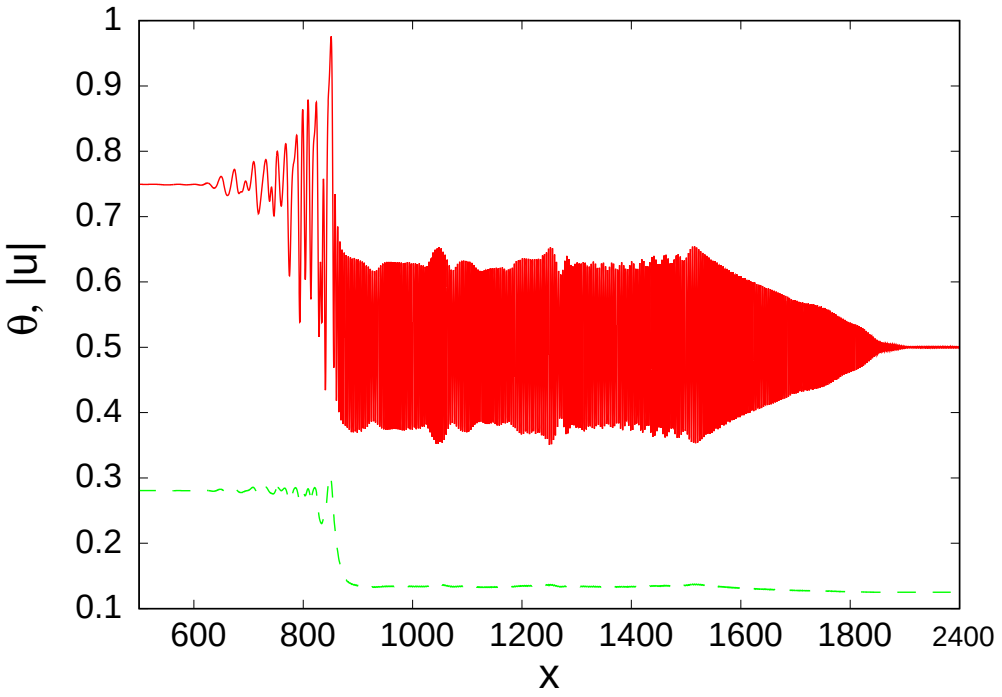


Figure 7: Numerical solutions of nematic equations (3) and (4) at $z = 1000$. Red (solid) lines: $|u|$; green (dashed) lines θ. Here $u_- = 1.0$, $u_+ = 0.5$, $q = 2$ and $\nu = 200$.

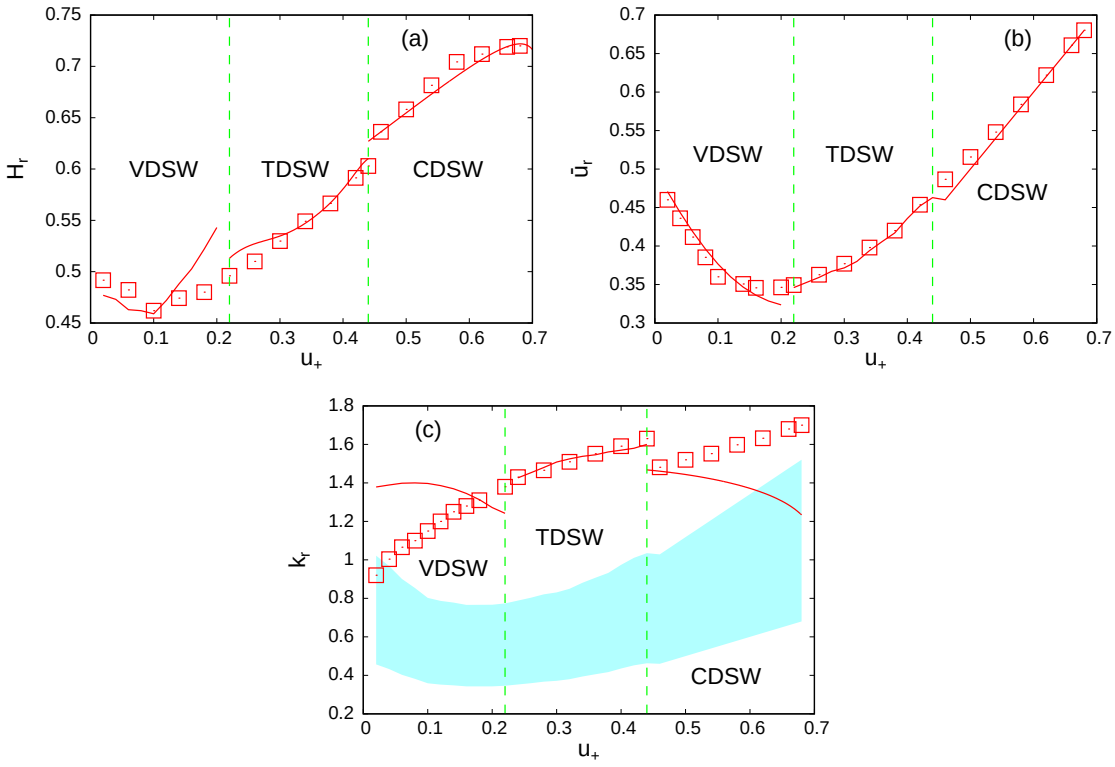


Figure 8: Resonant wavetrain parameters as given by numerical solutions of the nematic equations (3) and (4) and the DSW solutions for the CDSW, TDSW and VDSW regimes. Numerical solution: red boxes; analytical solution: red (solid) line. (a) height H_r of resonant wavetrain, (b) mean $\bar{u}_r$ of resonant wavetrain, (c) wavenumber k_r of resonant wavetrain. The blue (shaded) region is the region (49) of modulational stability for the resonant wave. Here $u_- = 1.0$, $\nu = 200$ and $q = 2$.

detailed figure also shows that the resonant wavetrain is non-uniform, in stark contrast with the resonant DSW solution of the 5th order KdV equation, equation (1) with $\mu = 0$, for which the resonant wavetrain has a constant amplitude with a front consisting of a partial DSW which takes the wavetrain down to the initial level u_+ ahead [29]. The same DSW structure as the present CDSW was found for the (unstable) DSW for the focusing NLS equation [68]. The DSW for this equation consists of a train of nearly equal amplitude waves, with a rapid decrease to the level u_- behind at the trailing edge. The work of [68] found that the major portion of unstable DSWs consists of a train of nearly equal amplitude waves, justifying the approximate theory of [69] which approximates DSWs as a train of equal amplitude solitary waves, with the amplitude, width and spacing of the solitary waves found from conservation laws, motivated by the work of [70] on the transcritical flow of a fluid over topography. The approximate method of [69] will then be used here to derive a solution for the nematic CDSW.

For simplicity, let us express the nematic KdV equation (20) as

$$\frac{\partial u_1}{\partial \eta} + B_2 u_1 \frac{\partial u_1}{\partial \xi} + B_3 \frac{\partial^3 u_1}{\partial \xi^3} + \epsilon^2 B_4 \frac{\partial^5 u_1}{\partial \xi^5} = 0, \tag{66}$$

where

$$B_2 = 3\sqrt{\frac{2}{q}}, \quad B_3 = \sqrt{\frac{2}{q}}\frac{u_+}{4}\left(\frac{\nu}{q} - \frac{q}{4u_+^2}\right), \quad B_4 = \sqrt{\frac{2}{q}}\frac{3\nu^2 u_+^2}{16q^2}. \tag{67}$$

This nematic KdV equation has the "mass" (optical power) conservation equation

$$\frac{\partial}{\partial\eta}u_1 + \frac{\partial}{\partial\xi}\left[\frac{1}{2}B_2 u_1^2 + B_3 u_{1\xi\xi} + \epsilon^2 B_4 u_{1\xi\xi\xi\xi}\right] = 0 \tag{68}$$

and the energy conservation equation

$$\frac{\partial}{\partial\eta}\frac{1}{2}u_1^2 + \frac{\partial}{\partial\xi}\left[\frac{1}{3}B_2 u_1^3 + B_3 u_1 u_{1\xi\xi} - \frac{1}{2}B_3 u_{1\xi}^2 + \epsilon^2 B_4 u_1 u_{1\xi\xi\xi\xi} - \epsilon^2 B_4 u_{1\xi} u_{1\xi\xi\xi} + \frac{1}{2}\epsilon^2 B_4 u_{1\xi\xi}^2\right] = 0. \tag{69}$$

These will now be used to find an approximate solution for the nematic CDSW by assuming that it consists of a uniform series of solitary waves [69], as discussed above.

Let us assume that the CDSW at position η consists of N equal solitary waves of amplitude $\tilde{a}_s$ and width $\tilde{w}_s$, where we shall use tildes to denote scaled variables in the moving and stretched coordinates (ξ, η). It is also assumed that the CDSW sheds a uniform resonant wavetrain of amplitude $\tilde{a}_r$ which propagates ahead of it. Then as $\xi \to -\infty$, $u_1 \to 1$ and as $\xi \to \infty$, $u_1 \to \tilde{a}_r \cos\left(\tilde{k}_r\xi - \tilde{\omega}_r\eta\right)$, since $|u| = u_+ + \epsilon^2 u_1$ with $\epsilon^2 = u_i - u_+$. Integrating the mass and energy equations (68) and (69) over the CDSW, we have

$$N\int_{-\infty}^{\infty} u_1\, d\xi = \left[\frac{1}{2}B_2 - \frac{1}{4}B_2\tilde{a}_r^2\right]\eta, \quad N\int_{-\infty}^{\infty}\frac{1}{2}u_1^2\, d\xi = \left[\frac{1}{3}B_2 - \frac{1}{4}\tilde{c}_g\tilde{a}_r^2\right]\eta. \tag{70}$$

In calculating the flux terms due to the resonant wavetrain on the right hand sides of (70), the averages of the resonant wavetrain and its square over a period have been used as the resonant wave is high frequency relative to the CDSW, see Figure 1(c). Also, $\tilde{c}_g$ is the group velocity of the shed radiation in the moving and stretched (ξ, η) coordinates. In calculating the energy conservation expression of (70) (the second) this group velocity is not that for the Kawahara equation (20), which is the group velocity for long waves in the nonlocal limit ν large, but that for the shed radiation, which is short wave radiation with the dispersion relation (14). It can be seen from these conservation relations that the shed radiation leaks mass and energy from the CDSW, which is the reason for the rapid decrease in its amplitude as u_+ decreases, as seen in Figure 2(a).

The integrals in the conservation expressions (70) are N times the integrals for a single solitary wave. Due to the high number of derivatives in the Kawahara equation (66), no exact solitary wave solutions have been derived for it. However, as for the PDSW solution of Section 4, the perturbation solution of [64, 71] which transforms the Kawahara equation to the standard KdV equation can be used to find a perturbed solitary wave solution of the Kawahara equation. This transformation gives that the solitary wave solution of (66) is

$$u_1 = \tilde{a}_s \operatorname{sech}^2\Theta - 5\epsilon^2 C_4\tilde{a}_s^2\operatorname{sech}^2\Theta + \frac{15}{2}\epsilon^2 C_4\tilde{a}_s^2\operatorname{sech}^4\Theta, \tag{71}$$

with the width $\tilde{w}_s$ of the solitary wave and its phase Θ given by

$$\tilde{w}_s = \frac{\sqrt{6B_3}}{\sqrt{B_2}}\frac{\sqrt{2}}{\sqrt{\tilde{a}_s}}, \quad \Theta = \frac{\xi - \tilde{V}_s\eta}{\tilde{w}_s}, \quad \tilde{V}_s = \frac{1}{3}B_2\tilde{a}_s\left(1 + 2\epsilon^2 C_4\tilde{a}_s\right). \tag{72}$$

With this perturbation solution for the solitary wave, the mass and energy of a single solitary wave can be calculated as

$$\int_{-\infty}^{\infty} u_1 \, d\xi = 2\tilde{a}_s \tilde{w}_s \tag{73}$$

and

$$\int_{-\infty}^{\infty} \frac{1}{2} u_1^2 \, d\xi = \frac{2}{3}\tilde{a}_s^2 \tilde{w}_s + \frac{4}{3}\epsilon^2 C_4 \tilde{a}_s^3 \tilde{w}_s, \tag{74}$$

respectively. Note that in the calculation of the energy, only terms up to $O(\epsilon^2)$ have been retained, consistent with the order of the transformation [64, 71]. Dividing the mass and energy relations (70) hence gives

$$\frac{1}{3}\tilde{a}_s + \frac{2}{3}\epsilon^2 C_4 \tilde{a}_s^2 = \frac{2}{3}\frac{1 - \frac{3}{4}\frac{\tilde{c}_g \tilde{a}_r^2}{B_2}}{1 - \frac{1}{2}\tilde{a}_r^2}. \tag{75}$$

Equation (75) determines the scaled amplitude $\tilde{a}_s$ of the solitary waves of the CDSW once the scaled amplitude $\tilde{a}_r$ of the shed resonant radiation is known. In a previous analysis of the nematic DSW a WKB solution for the shed resonant radiation was found which was found to be in excellent agreement with numerical solutions [42]. A WKB solution was used as the resonant wavetrain is short wave relative to the DSW. This solution for the resonant wavetrain was given in terms of the original variables u and (x, z). Returning the amplitude relation (75) to the original variables using $a_s = \epsilon^2 \tilde{a}_s = (u_i - u_+)\tilde{a}_s$ and $a_r = \epsilon^2 \tilde{a}_r = (u_i - u_+)\tilde{a}_r$ and using the resonant wavetrain solution of [42] gives that the amplitude of the CDSW solitary waves is determined by

$$a_s \left[1 + 2C_4 a_s\right] = 2\left(u_i - u_+\right) \frac{1 - \frac{3}{4}\frac{\left(c_g - \sqrt{\frac{2}{q}}\, u_+\right) a_r^2}{B_2 (u_i - u_+)^3}}{1 - \frac{1}{2}\frac{a_r^2}{(u_i - u_+)^2}}, \tag{76}$$

with the resonant radiation's amplitude a_r given by [42]

$$a_r = \frac{u_i - u_+}{1 + \frac{2u_+ k_r a_s}{q s_+ (k_r - s_+)^2}}. \tag{77}$$

Here the group velocity $c_g = k_r$, see (14) as $v_+ = 0$, has been used and the velocity of the solitary waves of the CDSW in the original variables is

$$s_+ = \sqrt{\frac{2}{q}}\, u_+ + \frac{1}{3} B_2 a_s \left(1 + 2C_4 a_s\right) \tag{78}$$

as the ξ frame moves with velocity $u_+\sqrt{2/q}$. The resonant wavenumber k_r is determined by the resonance condition (63). Equations (75) and (63), with (77), were solved numerically using Newton's method to determine the amplitude a_s and velocity s_+ of the solitary waves of the CDSW and the amplitude a_r and wavenumber k_r of the resonant wavetrain. It was found that the resonant wave amplitude a_r is negligible for $u_+ > 0.70$. This is then the upper limit of the CDSW regime, in excellent agreement with the upper CDSW regime limit of Table 1 found from numerical solutions. The lower limit of the CDSW regime will be discussed in the next section dealing with the TDSW regime.

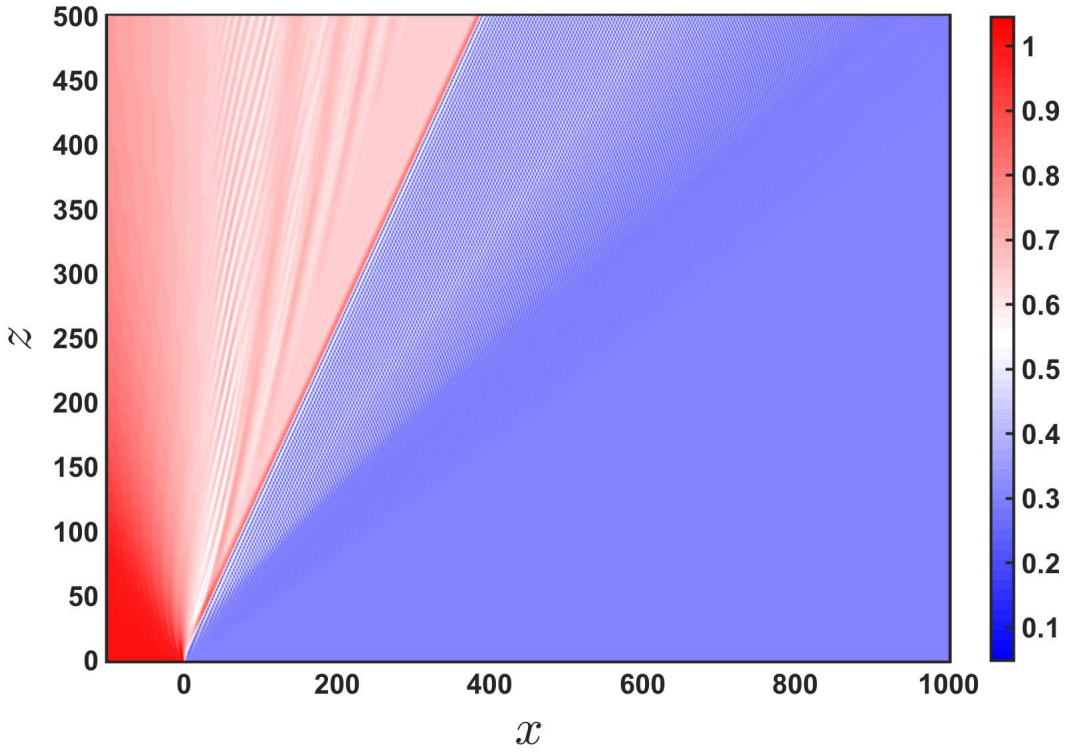


Figure 9: Numerical solution of the nematic equations (3) and (4) for $|u|$ in the TDSW regime showing the Whitham shock linking the resonant wavetrain with the intermediate shelf. Here $u_- = 1.0$, $u_+ = 0.3$, $\nu = 200$ and $q = 2$.

Figure 2(a) shows the height $H_s = u_+ + a_s + (5/2)C_4 a_s^2$ of the solitary waves of the CDSW (see (71)) as given by numerical solutions and the equal amplitude approximation of this section. It can be seen that there is excellent agreement, except near the boundary with the TDSW regime. This is expected since as the height of the jump $u_i - u_+$ grows, the KdV approximation becomes less valid. In addition, as the TDSW regime is approached, the form of the DSW changes fundamentally, with the waves of the DSW disappearing, except for one wave at the leading edge, see Figure 1(d). Figure 1(c) shows that the amplitudes of the individual waves of the CDSW have a random variation as the CDSW is unstable. To calculate H_s from the numerical solutions, an average was then taken over the CDSW, which is consistent with the equal amplitude approximation. Figure 2(a) shows a rapid decrease in the height of the CDSW as u_+ decreases. However, the amplitude a_r of the shed radiation grows, as can be seen from Figure 8(a), since $a_r = H_r - u_+$. The shed resonant radiation acts as a damping on the DSW and leads to its decay over the non-resonant PDSW case. Figure 2(b) shows comparisons for the velocity s_+ of the leading edge of the CDSW. The agreement is not as good as for the solitary wave height, but the difference between the numerical and analytical solutions is about 4%. There are no results presented for the trailing edge velocity, as for the PDSW and RDSW cases, as the equal amplitude approximation cannot give results for the linear trailing edge.

Figure 8(a) shows comparisons between numerical and analytical solutions for the height

$H_r = u_+ + a_r$ of the resonant wavetrain. There is again excellent agreement, as expected as the WKB solution was previously found to be in excellent agreement with numerical solutions [42]. It can be seen that as the RDSW regime is approached the amplitude $a_r = H_r - u_+$ of the resonant wavetrain goes to zero, as required. As discussed in Section 4 the resonant wavetrain in the CDSW regime is unstable when its amplitude is low and stabilises at high enough amplitude. For the comparisons of Figure 8(a) the amplitudes and heights of low amplitude numerical resonant waves were determined before instability broke the wavetrain up. In this regard, a unit distance in the non-dimensional variable z corresponds to about $2\mu m$ for optical beams in the near infrared [47, 48, 49]. Typical experimental nematic cell lengths are $\sim 1mm$, which is $z = 500$. As shown in Figure 5 the breakup of the resonant wavetrain in the vicinity of the CDSW occurs after $z = 1000$. This is well beyond the experimental distance at which optical solitary waves can be observed, due to their decay due to scattering losses [39, 40]. Numerical solutions show that the mean height of the resonant wavetrain is given by $\bar{u}_r = \sqrt{q\theta_r}$. The resonant wavetrain is rapidly varying. Averaging the director equation (4) then gives this mean height expression. Figure 8(b) shows a comparison between the mean height $\bar{u}_r$ of the resonant wavetrain as given by numerical solutions and by the theoretical CDSW value $\bar{u}_r = u_+$, with excellent agreement seen. Finally, Figure 8(c) shows comparisons for the wavenumber k_r of the resonant wavetrain. The numerical values of k_r were determined by averaging over the resonant wavetrain. Unlike the resonant wave height and mean level, the comparison is poor, except near the TDSW regime where the resonant wavetrain restabilises. The reason is that the resonant wavetrain is unstable over nearly all of the CDSW regime and does not consist of a single dominant wavenumber, as seen in Figures 5 and 6.

6 Nematic TDSW

As the initial level ahead u_+ decreases in the CDSW regime, the effect of the shed resonant wavetrain grows until the DSW itself ceases to exist and there is just a large amplitude resonant wavetrain with a small amplitude wave at its trailing edge linking it to the intermediate level, as shown in Figure 1(d). This is similar to the behaviour of the DSW for the Kawahara equation (1) for which the DSW ceases to exist for large enough initial steps (or small enough μ). The DSW is replaced by what is termed a TDSW, a travelling dispersive shock wave [29]. This work on the Kahawara equation shows that in the TDSW regime the DSW largely disappears, with a single remnant negative polarity solitary wave connecting the resonant wavetrain to the intermediate level u_i. The same structure is seen in Figure 1(d) for the nematic TDSW regime.

It was shown for the Kawahara equation that in the TDSW regime the resonant wavetrain is linked to the level u_+ ahead by a partial DSW [35]. A partial DSW is a modulated wavetrain which takes a uniform wavetrain down to a constant level, in contrast to a full DSW which is a modulated wavetrain which connects two uniform levels [72, 73]. As stated, a negative polarity solitary wave connects the resonant wavetrain to the level u_i behind [29]. As there is no known solitary wave solution of the Kawahara equation of either polarity, this connection was done numerically and by using approximate theory in previous work [29, 35]. However, it has been recently realised that the determination of this connecting negative polarity solitary wave is not necessary [36]. The connection between the resonant wavetrain and the level behind can be treated as a Whitham shock, the wavetrain equivalent of a gas dynamic shock, for the

Whitham modulation equations governing the resonant wavetrain, confirming speculation by Whitham when he originally developed modulation theory [1, 23]. This shock-like nature of the connection can be seen for the nematic TDSW illustrated in Figure 9, where the discontinuous connection between the resonant wave and the uniform level behind is clearly visible.

For the modulation equations to have a Whitham shock, they need to form a hyperbolic system. The Whitham modulation equations (45)–(48) for the Stokes' wave are hyperbolic in the restricted interval (49) and Figure 8(c) shows that the resonant wavetrain falls outside this region over nearly all the CDSW and all the TDSW existence intervals. However, as shown in Figure 1(d), the resonant wavetrain is stable in the TDSW regime. As discussed above, the Stokes' wave modulation equations are valid in the weakly nonlinear limit and the numerical results show that they do not correctly predict modulational stability for the resonant TDSW wave as it has relatively large amplitude. As the full Whitham modulation equations are not known, the Stokes' wave modulation equations will be used to find jump conditions for the connection between the intermediate level u_i and the resonant wavetrain in the TDSW regime.

As for the compressible gas equations, the appropriate modulation equations to determine the wave shock jump conditions are the mass (39), momentum (43) and energy equations (44) [1]. Consistent with the TDSW structure illustrated in Figure 1(d), ahead of the Whitham shock there is the resonant wavetrain with wavenumber $k = k_r$, mean height $\bar{u} = \bar{u}_r$ ($\bar{\rho} = \bar{\rho}_r = \bar{u}_r^2$), flow $\bar{v}_r$ and amplitude $a = a_r$. Behind the Whitham shock there is no wavetrain, so the wavenumber $k = 0$, the amplitude $a = 0$ and the mean height is $\bar{u} = u_i$. Let us denote the Whitham shock velocity by $U_{\rm shock}$. Then the mass (39), momentum (43) and energy (44) modulation equations give the jump conditions

$$-\left[\bar{\rho}_r - \rho_i\right] U_{\rm shock} + \left[\bar{\rho}_r\bar{v}_r + \frac{k_r a_r^2}{4\bar{\rho}_r} - \rho_i v_i\right] = 0, \tag{79}$$

$$-\left[\bar{\rho}_r\bar{v}_r + \frac{a_r^2 k_r}{4\bar{\rho}_r} - \rho_i v_i\right] U_{\rm shock} + \left[\frac{\bar{\rho}_r^2}{q} + \bar{v}_r^2\bar{\rho}_r + \frac{a_r^2 k_r^2}{4\bar{\rho}_r} + \frac{a_r^2\bar{v}_r k_r}{2\bar{\rho}_r} - \frac{\rho_i^2}{q} - v_i^2\rho_i\right] = 0, \tag{80}$$

and

$$-\left[\frac{2\bar{\rho}_r^2}{q} + \bar{v}_r^2\bar{\rho}_r + \frac{a_r^2 k_r^2}{4\bar{\rho}_r} + \frac{a_r^2\bar{v}_r k_r}{2\bar{\rho}_r} - \frac{2\rho_i^2}{q} - v_i^2\rho_i\right] U_{\rm shock}$$
$$+\left[\frac{4\bar{\rho}_r^2\bar{v}_r}{q} + \bar{\rho}_r\bar{v}_r^3 + \frac{a_r^2 k_r}{q} + \frac{3a_r^2 k_r^2\bar{v}_r}{4\bar{\rho}_r} + \frac{3a_r^2\bar{v}_r^2 k_r}{4\bar{\rho}_r} + \frac{a_r^2 k_r^3}{4\bar{\rho}_r} - \frac{4\rho_i^2 v_i}{q} - \rho_i v_i^3\right] = 0, \tag{81}$$

respectively [1]. Here, v_i on the intermediate level is related to ρ_i by (16) for the expansion wave solution from the initial level u_- behind. In addition, there is the resonance condition obtained from the Stokes' wave dispersion relation (25)

$$U_{\rm shock} = \bar{v}_r + \frac{1}{2}k_r + \frac{2\bar{\rho}}{qk_r} - \frac{k_r a_r^2}{8\bar{\rho}_r^2}. \tag{82}$$

These jump conditions and the resonance condition form four equations for the six unknown parameters ρ_i, $\bar{\rho}_r$, $\bar{v}_r$, k_r, a_r and $U_{\rm shock}$. For the fifth order KdV equation, (1) with $\mu = 0$, the system was completed by matching the resonant wavetrain to the partial DSW at its

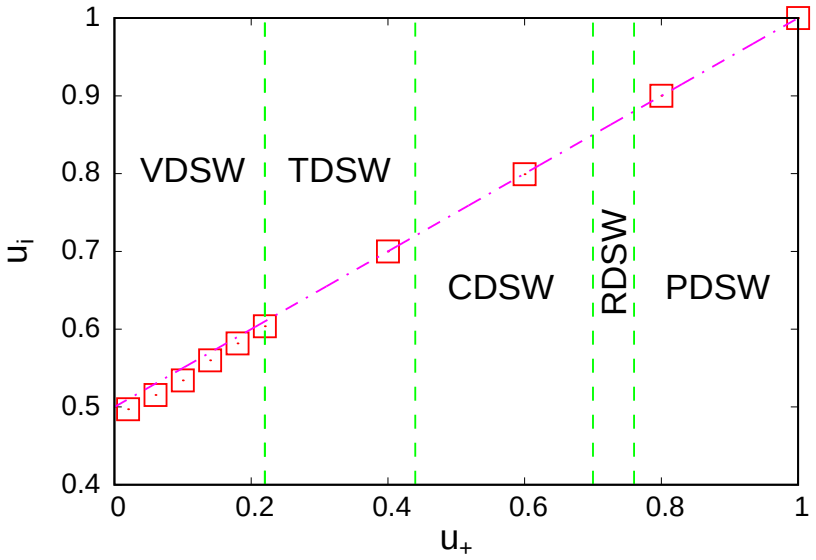


Figure 10: Intermediate level u_i as given by numerical solutions of the nematic equations (3) and (4), the Riemann invariant value (62) for the PDSW, RDSW, CDSW and TDSW regimes and the VDSW value (91). Numerical solution: red boxes; theoretical values: pink (dot-dashed) line. Here $u_- = 1.0$, $\nu = 200$ and $q = 2$.

leading edge, which brings the solution back to the level u_+. This partial bore was found as a simple wave solution of the modulation equations of the fifth order KdV equation in Riemann invariant form. Even when the Stokes' wave modulation equations are hyperbolic, they cannot be expressed in Riemann invariant form. So to complete the solution for the TDSW regime, some assumptions based on numerical solutions will be made.

Figure 10 shows the level u_i of the shelf between the expansion wave from u_- and the resonant wavetrain. It can be seen that in the TDSW regime, it is given by the average (62), $(1 + u_+)/2$ in this case, based on the conservation of the Riemann invariant R_- for the non-dispersive shallow water equations, given by (11), through the Whitham shock. The reason that this is an excellent approximation is that the Whitham shock is relatively weak, as seen from Figure 1(d), so that this Riemann invariant is conserved through the shock to leading order [1]. It will then be assumed that u_i is given by (62). Consistent with this, it is assumed from the shallow water Riemann invariant R_- given by (11) that

$$\bar{v}_r = 2\sqrt{\frac{2}{q}}\left(\sqrt{\bar{\rho}_r} - \sqrt{\rho_+}\right) = 2\sqrt{\frac{2}{q}}\left(\sqrt{\bar{\rho}_r} - u_+\right). \tag{83}$$

As noted in Section 3 the shallow water characteristics (47) and (48) are always real, so the Riemann invariants on these can be used to propagate the solution. This assumption is based on ignoring the wave amplitude correction in the Riemann variable (48) as this amplitude is small. With these assumptions, the jump conditions (79)–(81) were solved numerically using Newton's method.

Figures 8(a) and (b) give comparisons between numerical solutions and the results from the shock jump conditions for the resonant wave height $H_r = a_r + \bar{u}_r$ and the resonant wave mean level $\bar{u}_r$ in the TDSW regime. It can be seen that there is excellent agreement for

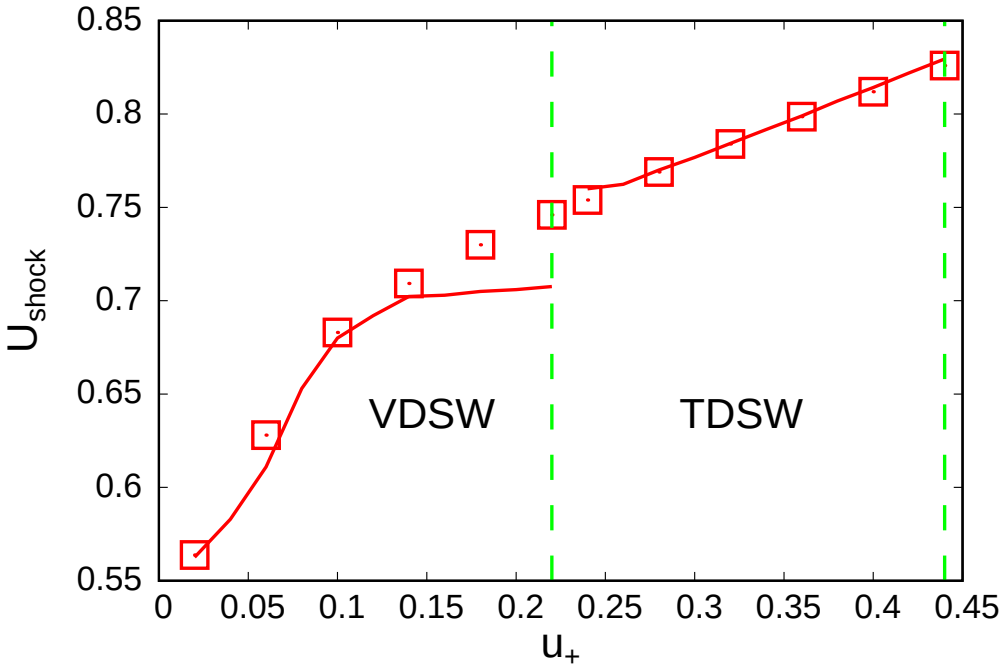


Figure 11: Modulation shock velocity $U_{\rm shock}$ in the TDSW and VDSW regimes as given by numerical solutions of the nematic equations (3) and (4) and the TDSW and VDSW regime solutions. Numerical solution: red boxes; analytical solution: red (solid) line. Here $u_- = 1.0$, $\nu = 200$ and $q = 2$.

both parameters with numerical solutions, with some slight deviation for the resonant wave height when it transitions to the VDSW regime. As for the equivalent transitions for the CDSW regime, this is to be expected as the resonant wave drastically changes form in the VDSW regime, as seen from Figure 1(e). Figure 8(c) shows a comparison for the resonant wavenumber k_r and nearly perfect agreement across the TDSW regime is seen, unlike for the CDSW regime. The higher resonant wave amplitude in the TDSW regime has stabilised the wavetrain, so that the assumption of a single dominant resonant wavenumber is now valid. For $u_+ > 0.44$, the Whitham shock velocity $U_{\rm shock}$ is greater than the (linear) group velocity c_g of the resonant wavetrain, which is unphysical. This value of u_+ is then the boundary between the TDSW and CDSW regimes, in excellent agreement with numerical results, as tabulated in Table 1.

Figure 11 shows a comparison between numerical solutions and the Whitham shock jump conditions for the shock velocity $U_{\rm shock}$. Again there is near perfect agreement, except for a slight deviation near the transition to the VDSW regime. This excellent agreement for the TDSW parameters validates the assumptions (62) and (83) made above.

7 Nematic Vacuum DSW

As the level ahead u_+ decreases in the TDSW regime, the resonant wavetrain hits the vacuum point at which $\bar{u}_r - a_r = 0$, at which point the DSW changes form [50, 74]. When this critical level is reached, the DSW changes to the vacuum DSW (VDSW) regime, with Figure 1(e)

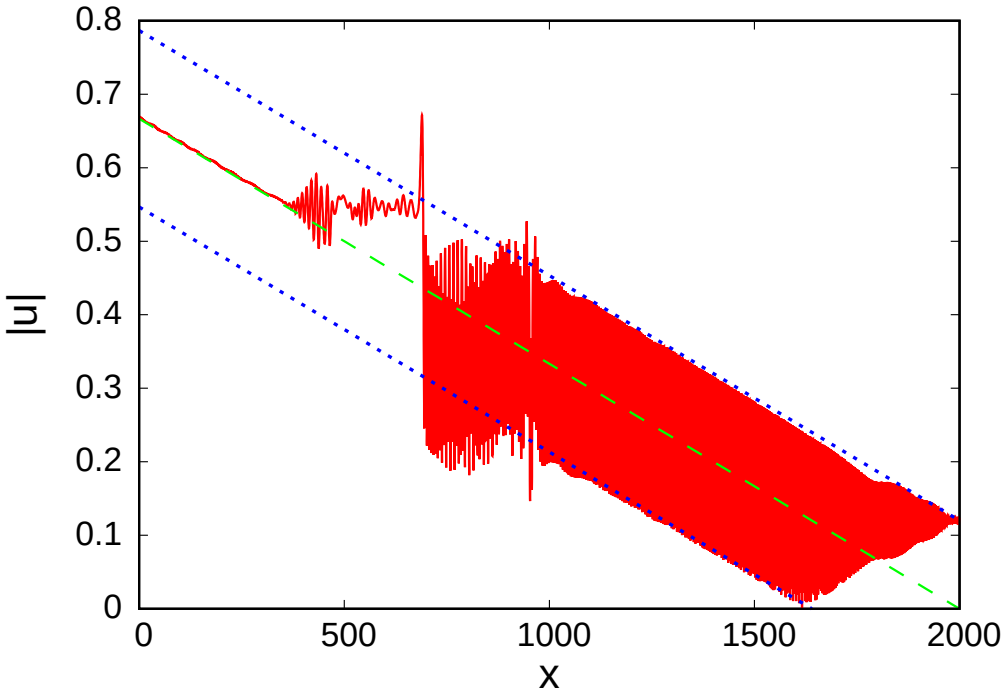


Figure 12: Numerical solution of the nematic equations (3) and (4) for $|u|$: red (solid) line; expansion wave solution (15): green (dashed) line; expansion wave solution (15) $\pm u_+$: blue (dotted) line, $+u_+$ (upper), $-u_+$ (lower). Here $u_- = 1.0$, $u_+ = 0.12$, $\nu = 200$ and $q = 2$.

showing a typical VDSW solution. Table 1 shows this critical value of u_+ for the vacuum point as given by the jump conditions (79)–(81) and by numerical solutions, with excellent agreement seen. The partial DSW of the TDSW regime which brings the resonant wavetrain down to u_+ is now on a (linearly) varying mean. As for the TDSW regime, there is a Whitham shock which links the resonant wavetrain to the intermediate level u_i, so that this will be determined by the same jump conditions as for the TDSW regime. As for the TDSW regime, some assumptions based on numerical solutions will need to be made to derive the VDSW solution due to the lack of Whitham modulation equations in Riemann invariant form.

Figure 12 shows an expanded version of the VDSW solution of Figure 1(e). On the same figure the expansion wave solution (15) continued down to $u = 0$ and this solution with $\pm u_+$ added are shown. It can be seen that the mean and envelopes of the transition wave bringing the resonant wavetrain down to u_+ from the intermediate shelf are well approximated by this expansion wave solution. This type of wavetrain structure does not exist for the NLS DSW in the vacuum case as there is no resonance [50]. Without full Whitham modulation equations for the fully nonlinear nematic equations, there is no analytical method to justify this observed structure. This structure will be assumed here, with some justification based on weak shock theory.

Figure 12 shows that the resonant wavetrain and its leading edge have constant amplitudes, so that $a_r = u_+$ will be assumed, which is consistent with the wave envelopes of this figure. The resonant wave amplitude is small, so that it decouples from the mean height variation in the modulation equations. As the resonant wave amplitude is small, it will be ignored in the modulation equations (45)–(48), so that the modulation equations (47) and (48) become

the shallow water equations [1]. The jump conditions of Section 6 then become the shallow water equation jump conditions, for which the most convenient form is [1]

$$U_{\rm shock} = \bar{v}_r \pm \sqrt{\frac{2}{q}} \left[\frac{u_i^2 \left(u_i^2 + \bar{u}_r^2\right)}{2\bar{u}_r^2} \right]^{1/2}, \quad v_i = \bar{v}_r \pm \sqrt{\frac{2}{q}} \frac{u_i^2 - \bar{u}_r^2}{u_i^2} \left[\frac{u_i^2 \left(u_i^2 + \bar{u}_r^2\right)}{2\bar{u}_r^2} \right]^{1/2}. \tag{84}$$

The sign choice for the shallow water equations (and the compressible gas equations) is the + sign. However, with this choice, in the limit $u_+ \to 0$, the shock velocity approaches the front velocity of the dam break solution $2u_-\sqrt{2/q}$, and $u_i \to 0$. This does not accord with numerical solutions, which show that $u_i \to u_-/2$ in this limit, which is the Riemann invariant value (62). The correct behaviour is obtained with the − sign choice in the shallow water jump conditions (84). Figure 12 also shows that the Whitham shock is weak, the jump is small. Expanding the jump conditions (84) for small jump height, $|u_i - \bar{u}_r|$ small, gives

$$U_{\rm shock} = \bar{v}_r - \sqrt{\frac{2}{q}} \bar{u}_r \left[1 + \frac{3}{4} \frac{u_i^2 - \bar{u}_r^2}{\bar{u}_r^2} - \frac{9}{32} \frac{\left(u_i^2 - \bar{u}_r^2\right)^2}{\bar{u}_r^4} + \ldots \right], \tag{85}$$

$$v_i = \bar{v}_r - \sqrt{\frac{2}{q}} \frac{u_i^2 - \bar{u}_r^2}{\bar{u}_r} \left[1 - \frac{u_i^2 - \bar{u}_r^2}{4\bar{u}_r^2} + \ldots \right]. \tag{86}$$

We see from the upper expansion wave envelope in Figure 12 and the expansion wave solution (15) that

$$u_i = \frac{\sqrt{q}}{3\sqrt{2}} \left(\frac{2\sqrt{2}}{\sqrt{q}} u_- - U_{\rm shock} \right) + u_+, \tag{87}$$

so that

$$U_{\rm shock} = 2\sqrt{\frac{2}{q}} u_- + 3\sqrt{\frac{2}{q}} \left(u_+ - u_i\right). \tag{88}$$

As for the TDSW solution, the shallow water Riemann variables (47) and (48) will be used to propagate the solution. Furthermore, as for the TDSW regime, the amplitude corrections to these Riemann variables will be neglected, so that they become the Riemann invariants (10) and (11). As the shock is weak, at leading order the Riemann invariant R_+ (10) is conserved through the shock, so that at first order, that is shock strength zero,

$$2\sqrt{\frac{2}{q}} u_- = \bar{v}_r + 2\sqrt{\frac{2}{q}} \bar{u}_r. \tag{89}$$

A measure of the shock strength is u_+ as it is small. We then seek a weak shock correction to this Riemann invariant as

$$\bar{v}_r + 2\sqrt{\frac{2}{q}} \bar{u}_r = 2\sqrt{\frac{2}{q}} \left(u_- + \delta_1 u_+ + \delta_2 u_+^2 + \ldots \right). \tag{90}$$

Substituting the Riemann invariant correction (90) and the assumed upper envelope expression (88) into the weak shock jump conditions (85) and (86) and solving as a series in small u_+, we find $\delta_1 = \delta_2 = 0$ and

$$u_i = \bar{u}_r + 2u_+ - \frac{u_+^2}{\bar{u}_r}. \tag{91}$$

To $O(u_+^2)$ there is then no correction to the shallow water Riemann invariant. Equation (88) then gives the Whitham shock velocity. As the Riemann invariant R_+ is conserved to $O(u_+^2)$ through the weak Whitham shock, the intermediate level result (62) holds to $O(u_+^2)$, as confirmed from the intermediate level comparison of Figure 10. Using this intermediate level expression in the shock result (91) gives that

$$\bar{u}_r = \frac{1}{4}u_- - \frac{3}{4}u_+ + \frac{1}{4}\sqrt{u_-^2 - 6u_+u_- + 25u_+^2} = \frac{1}{2}u_- - \frac{3}{2}u_+ + \frac{2u_+^2}{u_-} + \dots \tag{92}$$

Figure 11 shows comparisons between numerical solutions for the Whitham shock velocity with the result (88) in the VDSW regime. It can be seen that there is excellent agreement, except near the transition to the TDSW regime where the DSW form changes. As the transition to the TDSW regime is approached, the amplitude of the resonant wavetrain increases, so that its neglect in the Riemann variables becomes less valid.

Figure 8(a) gives comparisons for the height $H_r = a_r + \bar{u}_r = u_+ + \bar{u}_r$ of the resonant wavetrain with numerical values. Again, there is good agreement, except near the transition to the TDSW regime, again because the neglect of the resonant wave amplitude correction to the Riemann variables becomes less accurate. The resonant wavetrain mean $\bar{u}_r$ comparison of Figure 8(b) is similar, with excellent comparison. Figure 10 shows an excellent comparison between the numerical mean level u_i in the VDSW regime and the VDSW result (91), as expected as the Riemann invariant R_+ is conserved to $O(u_+^2)$ through the weak Whitham shock. Finally, Figure 8(c) shows comparisons for the resonant wavenumber k_r. As for the CDSW regime, the agreement is poor, except near the boundary with the TDSW regime where the resonant wavetrain restabilises due to its increased amplitude. As stated, it was found that the Riemann invariant R_+ (10) is conserved to $O(u_+^2)$ through the Whitham shock, which means that the intermediate level u_i is given by the mean value (62) to this order. It can be seen from Figure 10 that there is a slight deviation in u_i from the mean value in the VDSW regime which grows as u_+ decreases. Presumably, this deviation is due to higher order corrections in the Riemann invariant expansion (90). As this correction is small, it is not considered here.

8 Dependence on Initial Wavenumber

The analysis and comparisons of the previous sections were for initial jumps (5) with zero wavenumber $v_- = v_+ = 0$. The effect of initial wavenumber on the development of DSWs for the defocusing NLS equation has been investigated and it was found that solutions consist of a combination of DSWs and (non-dispersive) expansion waves [50]. In detail, there are six distinct types of solutions for the defocusing NLS equation. The situation for the nematic equations (3) and (4) is more complicated, as can be seen from the DSW types illustrated in Figure 1 for $v_- = v_+ = 0$. There are multiple DSW types, depending on the height of the initial jump, so that for each defocusing NLS solution with a DSW, there are five such solutions for the nematic equations. To finish the analysis of DSW solutions for the nematic equations, the broad extra five types of solution for the nematic equations will be briefly discussed, with the solutions for each of these types briefly outlined as the details are similar to those derived in the previous sections for $v_- = v_+ = 0$. The new general types of solutions, consisting of various combinations of DSWs and expansion waves (solutions of the shallow water equations (10) and (11)) are illustrated in Figure 13.

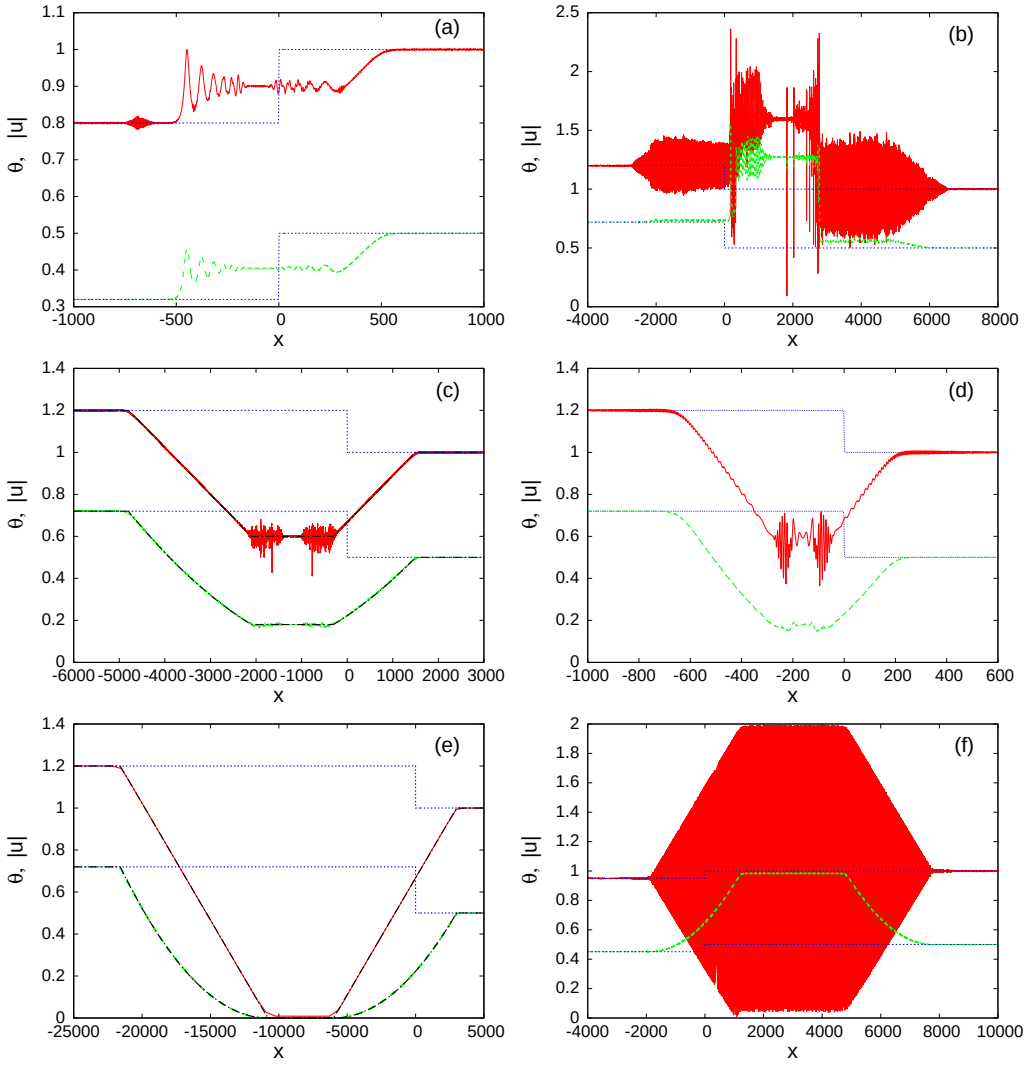


Figure 13: Numerical solutions of the nematic equations (3) and (4) for the initial condition (5). Red (solid) lines: $|u|$; green (dashed) lines θ; blue (dotted) lines: $|u|$ at $z = 0$ (upper) and θ at $z = 0$ (lower). (a) $u_- = 0.8$, $u_+ = 1.0$, $v_- = 0$, $v_+ = 0$, $z = 500$ (b) $u_- = 1.2$, $u_+ = 1.0$, $v_- = 2$, $v_+ = 0$, $z = 1500$, (c) $u_- = 1.2$, $u_+ = 1.0$, $v_- = -2.0$, $v_+ = 0$, $z = 1500$, black (dash-dot) line: expansion wave solution (94), (d) $u_- = 1.2$, $u_+ = 1.0$, $v_- = -2.0$, $v_+ = 0$, $z = 200$, (e) $u_- = 1.2$, $u_+ = 1.0$, $v_- = -6.0$, $v_+ = 0.0$, $z = 1500$, black (dash-dot) line: expansion wave solution (94), (f) $u_- = 0.95$, $u_+ = 1.0$, $v_- = 6.0$, $v_+ = 0$, $z = 1000$. Here $\nu = 200$ and $q = 2$.

The simplest case is the reversal of the orientation of the initial jump, $u_- < u_+$, with $u_- < u_i < u_+$, as shown in Figure 13(a). As the nematic equations are bidirectional, the solutions for this case are just the solutions of the previous sections, but reversed in direction.

The mean height (62), valid for the initial condition (5) with no wavenumber jump, can be extended to include such a jump, resulting in

$$u_i = \frac{1}{2}\left(u_- + u_+\right) + \frac{1}{4}\frac{\sqrt{q}}{\sqrt{2}}\left(v_- - v_+\right), \tag{93}$$

which is obtained by propagating the rear conditions u_-, v_- on the characteristics C_+ (10) and the front conditions u_+, v_+ on the characteristics C_- (11). A more substantive example than that of Figure 13(a) is shown in Figure 13(b). This example shows two DSWs, both crossover cases, preceded by large resonant wavetrains. This case arises when $u_i > u_- > u_+$, which results in two DSWs. These CDSWs and resonant wavetrains can be analysed using the approximate method of Section 5.

When $0 < u_i < u_+$, two expansion waves are generated due to the change in orientation of the jumps between the initial states u_- and u_+ and the intermediate level. One expansion wave is a generalisation of (15) with $v_-, v_+ \neq 0$. The other is the equivalent simple wave solution on the characteristic C_+ (10) with the Riemann invariant R_- (11) constant through the expansion fan. This results in the solution

$$|u| = \begin{cases} u_-, & \frac{x}{z} < v_- - \frac{\sqrt{2}}{\sqrt{q}}u_- \\ \frac{\sqrt{q}}{3\sqrt{2}}\left[v_- + \frac{2\sqrt{2}}{\sqrt{q}}u_- - \frac{x}{z}\right], & v_- - \frac{\sqrt{2}}{\sqrt{q}}u_- \leq \frac{x}{z} \leq \frac{1}{4}\left(v_- + 3v_+\right) + \frac{1}{2}\frac{\sqrt{2}}{\sqrt{q}}\left(u_- - 3u_+\right), \\ u_i = \frac{1}{2}\left(u_- + u_+\right) + \frac{1}{4}\frac{\sqrt{q}}{\sqrt{2}}\left(v_- - v_+\right), & \frac{1}{4}\left(v_- + 3v_+\right) + \frac{1}{2}\frac{\sqrt{2}}{\sqrt{q}}\left(u_- - 3u_+\right) < \frac{x}{z} \\ & < \frac{1}{4}\left(3v_- + v_+\right) + \frac{1}{2}\frac{\sqrt{2}}{\sqrt{q}}\left(3u_- - u_+\right), \\ \frac{\sqrt{q}}{3\sqrt{2}}\left[\frac{2\sqrt{2}}{\sqrt{q}}u_+ - v_+ + \frac{x}{z}\right], & \frac{1}{4}\left(3v_- + v_+\right) + \frac{1}{2}\frac{\sqrt{2}}{\sqrt{q}}\left(3u_- - u_+\right) \leq \frac{x}{z} \leq v_+ + \frac{\sqrt{2}}{\sqrt{q}}u_+, \\ u_+, & v_+ + \frac{\sqrt{2}}{\sqrt{q}}u_+ < \frac{x}{z} \end{cases} \tag{94}$$

and

$$v = \begin{cases} v_-, & \frac{x}{z} < v_- - \frac{\sqrt{2}}{\sqrt{q}}u_- \\ \frac{1}{3}v_- + \frac{2}{3}\frac{\sqrt{2}}{\sqrt{q}}u_- + \frac{2}{3}\frac{x}{z}, & v_- - \frac{\sqrt{2}}{\sqrt{q}}u_- \leq \frac{x}{z} \leq \frac{1}{4}\left(v_- + 3v_+\right) + \frac{1}{2}\frac{\sqrt{2}}{\sqrt{q}}\left(u_- - 3u_+\right), \\ v_i = \frac{1}{2}\left(v_- + v_+\right) + \frac{\sqrt{2}}{\sqrt{q}}\left(u_- - u_+\right), & \frac{1}{4}\left(v_- + 3v_+\right) + \frac{1}{2}\frac{\sqrt{2}}{\sqrt{q}}\left(u_- - 3u_+\right) < \frac{x}{z} \\ & < \frac{1}{4}\left(3v_- + v_+\right) + \frac{1}{2}\frac{\sqrt{2}}{\sqrt{q}}\left(3u_- - u_+\right), \\ \frac{1}{3}v_+ - \frac{2}{3}\frac{\sqrt{2}}{\sqrt{q}}u_+ + \frac{2}{3}\frac{x}{z}, & \frac{1}{4}\left(3v_- + v_+\right) + \frac{1}{2}\frac{\sqrt{2}}{\sqrt{q}}\left(3u_- - u_+\right) \leq \frac{x}{z} \leq v_+ + \frac{\sqrt{2}}{\sqrt{q}}u_+, \\ v_+, & v_+ + \frac{\sqrt{2}}{\sqrt{q}}u_+ < \frac{x}{z}, \end{cases} \tag{95}$$

which consists of two expansion fans either side of the intermediate level u_i. The corresponding director solution is given by $\theta = |u|^2/q$. This expansion wave solution is compared with a numerical solution in Figure 13(c), with near perfect agreement seen. The main disagreement is the high frequency dispersive waves at the junctions of the expansion fans and the intermediate level u_i, which are not captured by the non-dispersive expansion waves. The origin of these dispersive waves can be seen from Figure 13(d), which is the same solution as in Figure 13(c), but at a lower value $z = 200$, rather than $z = 1500$. As the initial condition pushes

down to create the intermediate level u_i, two small jumps in the centre of the intermediate level are created, which generate small DSWs. As the DSWs are resonant, resonant diffractive waves are also created, which is the origin of the diffractive waves in Figure 13(c).

This expansion fan solution holds until the vacuum case is reached, $u_i \leq 0$, so that (94) becomes invalid. However, the expansion wave solution (94) is valid if in the sections for which $|u|$ is negative, the solution is replaced by $|u| = 0$. Such a comparison is shown in Figure 13(e) and it can be seen that the comparison is excellent, as for that of Figure 13(c).

The final generic DSW solution is that illustrated in Figure 13(f). This solution occurs when the two DSWs of Figure 13(b) collide and interact, as for the equivalent case for the NLS equation [75]. The solution for this regime is then a two phase wavetrain, which is difficult to analyse without the full Whitham modulation equations. The particular solution shown in Figure 13(f) is two interacting TDSWs. There are two partial DSWs on either side of the central wavetrain, which is a (stable) uniform resonant wavetrain. In essence, the interaction has destroyed the intermediate level so that the two individual TDSWs can join. It is difficult to give the range of validity in (u_+, u_-, v_+, v_-) for this case as the borderline occurs when the tails of the two DSWs interact, noting that the velocities of the trailing edges of the DSWs critically depend on which regimes they lie in.

9 Conclusions

Dispersive shock wave (DSW) solutions of the nematic equations (3) and (4) have been found in the high nonlocality limit $\nu \gg 1$, which is the experimentally relevant limit [39, 40]. It was found that there are six distinct DSW types, see Figure 1. In contrast to previous work [41, 42] the solutions in these six regimes were found based on different asymptotic and approximate techniques appropriate for each regime. The work of [41] assumed that the DSW was of KdV type in all regimes, except the dam break case, while that of [42] assumed that the DSW solution was determined by a gas dynamics type shock, except in the dam break case. The present work shows that the nematic DSW is more complicated than this, with the PDSW and TDSW regimes consisting of (perturbed) KdV-type DSWs and the TDSW and VDSW regimes being determined by Whitham shocks in the appropriate Whitham modulation equations. The CDSW regime is a transition between these two broad types. One novel feature of the present work is the use of Whitham shocks for Whitham modulation equations, as pioneered by [36], validating ideas of Whitham [1, 23] when he first developed modulation theory. The nematic DSW shows a wider range of behaviours and solution types than the equivalent resonant Kawahara DSW [29, 35]. The DSW solutions for all six regimes show excellent agreement with numerical solutions for the DSW itself (when it exists), the resonant wavetrain (when it exists) and the intermediate level linking the backwards propagating expansion wave with the DSW or Whitham shock. The only exception is for the wavenumber of the resonant wavetrain when this wavetrain is unstable, as would be expected.

As stated, the present work obtained solutions for the nematic DSW in the highly nonlocal limit $\nu \gg 1$. As can be seen from Figures 1(a) and 4 the form of the DSW is highly dependent on the value of ν. Indeed, the nematic equations (3) and (4) reduce to the defocusing NLS equation for $\nu = 0$ and a perturbed defocusing NLS equation for ν small, for which there is no resonance. It is then of interest to study the transition from the highly nonlocal case to the local case with ν small. In this regard, the DSW changes from resonant to non-resonant, as

indicated by the change of sign of the third derivative of the small deviation KdV reduction (20) of the nematic equations.

Most of the solutions for the DSW types derived here have been based to a greater or lesser degree on the Whitham modulation equations for the periodic wave solution of the nematic equations. Unfortunately, this periodic wave solution is not known in general and a weakly nonlinear Stokes' wave approximation was used. While this generally gave satisfactory results, the Whitham modulation equations based on it gave incorrect modulational stability when the wave amplitude was not small. Whether these weakly nonlinear modulation equations can be improved on is not clear.

As stated in Section 2, the nematic system (3) and (4) is general and applies to other nonlinear optical media. In particular, for optical thermal media $q = 0$ in the director equation (4) is a physical limit, in which case θ is the temperature of the medium. In this limit, $|u|$ constant ceases to be a valid solution of the system, so that the step initial condition (5) does not result in an expansion wave and DSW being generated between the initial levels u_- and u_+. The form of a DSW for $q = 0$ is an open question.

In summary, while the form of the DSW in the highly nonlocal limit has been largely resolved, there are still many open questions in regard to DSW solutions of the nematic system for general nonlocality and other parameter values.

Saleh Baqer thanks Kuwait University for a scholarship to undertake his Ph.D. at the University of Edinburgh. The authors thank Côme Houdeville for pointing out errors in the manuscript.

References

[1] G.B. Whitham, *Linear and Nonlinear Waves,* J. Wiley and Sons, New York (1974).

[2] A.C. Newell, *Solitons in Mathematics and Physics,* SIAM, Philadelphia (1985).

[3] G.A. El and M.A. Hoefer, "Dispersive shock waves and modulation theory," *Physica D,* **333**, 11–65 (2016).

[4] R.S. Johnson, "A non-linear equation incorporating damping and dispersion," *J. Fluid Mech.,* **42**, 49–60 (1970).

[5] D.R. Christie, "Long nonlinear waves in the lower atmosphere," *J. Atmos. Sci.,* **46**, 1462–1491 (1989).

[6] R.H. Clarke, R.K. Smith and D.G. Reid, "The morning glory of the Gulf of Carpentaria: an atmospheric undular bore," *Monthly Weather Rev.,* **109**, 1726–1750 (1981).

[7] V.A. Porter and N.F. Smyth, "Modelling the Morning Glory of the Gulf of Carpentaria," *J. Fluid Mech.,* **454**, 1–20 (2002).

[8] N.F. Smyth and P.E. Holloway, "Hydraulic jump and undular bore formation on a shelf break," *J. Phys. Ocean.,* **18**, 947–962 (1988).

[9] P.G. Baines, *Topographic Effects in Stratified Flows,* Cambridge Monographs on Mechanics, Cambridge (1995).

[10] J.G. Esler and J.D. Pearce, "Dispersive dam-break and lock-exchange flows in a two-layer fluid," *J. Fluid Mech.,* **667**, 555–585 (2011).

[11] D.R. Scott and D.J. Stevenson, "Magma solitons," *Geophys. Res. Lett.,* **11**, 1161–1164 (1984).

[12] D.R. Scott and D.J. Stevenson, "Magma ascent by porous flow," *Geophys. Res. Lett.,* **91**, 9283–9296 (1986).

[13] N.K. Lowman and M.A. Hoefer, "Dispersive shock waves in viscously deformable media," *J. Fluid Mech.,* **718**, 524–557 (2013).

[14] T.R. Marchant and N.F. Smyth, "Approximate solutions for magmon propagation from a reservoir," *IMA J. Appl. Math.,* **70**, 796–813 (2005).

[15] C. Barsi, W. Wan, C. Sun and J.W. Fleischer, "Dispersive shock waves with nonlocal nonlinearity," *Opt. Lett.,* **32**, 2930–2932 (2007).

[16] W. Wan, S. Jia and J.W. Fleischer, "Dispersive superfluid-like shock waves in nonlinear optics," *Nature Phys.,* **3**, 46–51 (2007).

[17] G.A. El, A. Gammal, E.G. Khamis, R.A. Kraenkel and A.M. Kamchatnov, "Theory of optical dispersive shock waves in photorefractive media," *Phys. Rev. A,* **76**, 053183 (2007).

[18] G. Xu, A. Mussot, A. Kudlinski, S. Trillo, F. Copie and M. Conforti, "Shock wave generation triggered by a weak background in optical fibres," *Opt. Lett.,* **41**, 2656–2659 (2016).

[19] G.A. El, A.M. Kamchatnov, V.V. Khodorovskii, E.S. Annibale and A. Gammal, "Two-dimensional supersonic nonlinear Schrdinger flow past an extended obstacle," *Phys. Rev. E,* **80**, 046317 (2009).

[20] N.K. Lowman and M.A. Hoefer, "Fermionic shock waves: Distinguishing dissipative versus dispersive resolutions," *Phys. Rev. A,* **88**, 013605 (2013).

[21] X. An, T.R. Marchant and N.F. Smyth, "Optical dispersive shock waves in defocusing colloidal media," *Physica D,* **342**, 45–56 (2017).

[22] G.B. Whitham, "A general approach to linear and non-linear dispersive waves using a Lagrangian," *J. Fluid Mech.,* **22**, 273–283 (1965).

[23] G.B. Whitham, "Non-linear dispersive waves," *Proc. Roy. Soc. London A,* **283**, 238–261 (1965).

[24] G.B. Whitham, "Variational methods and applications to water waves," *Proc. Roy. Soc. London A,* **299**, 6–25 (1967).

[25] A.V. Gurevich and L.P. Pitaevskii, "Nonstationary structure of a collisionless shock wave," *Sov. Phys. JETP,* **33**, 291–297 (1974).

[26] H. Flaschka, M.G. Forest and D.W. McLaughlin, "Multiphase averaging and the inverse spectral solution of the Korteweg-de Vries equation," *Comm. Pure Appl. Math.,* **33**, 739–784 (1980).

[27] G.A. El, "Resolution of a shock in hyperbolic systems modified by weak dispersion," *Chaos,* **15**, 037103 (2005).

[28] T. Kawahara, "Oscillatory solitary waves in dispersive media," *J. Phys. Soc. Jpn.,* **33**, 260–264 (1972).

[29] P. Sprenger and M.A. Hoefer, "Shock waves in dispersive hydrodynamics with nonconvex dispersion," *SIAM J. Appl. Math.,* **77**, 26–50 (2017).

[30] M. Conforti and S. Trillo, "Dispersive wave emission from wave breaking," *Opt. Lett.,* **38**, 3815–3818 (2013).

[31] M. Conforti and S. Trillo, "Radiative effects driven by shock waves in cavity-less four-wave mixing combs," *Opt. Lett.,* **39**, 5760–5763 (2014).

[32] M. Conforti, S. Trillo, A. Mussot and A. Kudlinski, "Parametric excitation of multiple resonant radiations from localized wavepackets," *Sci. Rep.,* **5**, 1–5 (2015).

[33] S. Malaguti, M. Conforti and S. Trillo, "Dispersive radiation induced by shock waves in passive resonators," *Opt. Lett.,* **39**, 5626–5629 (2014).

[34] Y.S. Kivshar and G.P. Agrawal, *Optical Solitons. From Fibers to Photonic Crystals,* Academic Press, San Diego (2003).

[35] M.A. Hoefer, N.F. Smyth and P. Sprenger, "Modulation theory solution for nonlinearly resonant, fifth-order Korteweg-de Vries, nonclassical, travelling dispersive shock waves," *Stud. Appl. Math.,* **142**, 219–240 (2019).

[36] P. Sprenger and M.A. Hoefer, "Discontinuous shock solutions of the Whitham modulation equations and traveling wave solutions of higher order dispersive nonlinear wave equations," submitted for publication, arXiv: 1907.09329.

[37] S. Gavrilyuk, B. Nkonga, K.-M. Shyue and L. Truskinovsky, "Generalized Riemann problem for dispersive equations," hal-01958328 (2018).

[38] I.C. Khoo, *Liquid Crystals: Physical Properties and Nonlinear Optical Phenomena,* Wiley, New York (1995).

[39] M. Peccianti and G. Assanto, "Nematicons," *Phys. Rep.,* **516**, 147–208 (2012).

[40] G. Assanto, "Nematicons: reorientational solitons from optics to photonics," *Liquid Cryst. Reviews,* **6**, 170–194 (2018).

[41] N.F. Smyth, "Dispersive shock waves in nematic liquid crystals," *Physica D*, **333**, 301–309 (2016).

[42] G.A. El and N.F. Smyth, "Radiating dispersive shock waves in non-local optical media," *Proc. Roy. Soc. Lond. A,* **472**, 20150633 (2016).

[43] M. Peccianti, G. Assanto, A. De Luca, C. Umeton and I.C. Khoo, "Electrically assisted self-confinement and waveguiding in planar nematic liquid crystal cells," *Appl. Phys. Lett.,* **77**, 7–9 (2000).

[44] A. Piccardi, A. Alberucci, N. Tabiryan and G. Assanto, "Dark nematicons," *Opt. Lett.,* **36**, 1356–1358 (2011).

[45] C. Conti, M. Peccianti and G. Assanto, "Route to nonlocality and observation of accessible solitons," *Phys. Rev. Lett.,* **91**, 073901 (2003).

[46] G. Assanto, A. A. Minzoni, M. Peccianti and N. F. Smyth, "Optical solitary waves escaping a wide trapping potential in nematic liquid crystals: modulation theory," *Phys. Rev. A,* **79**, 033837 (2009).

[47] U.A. Laudyn, M. Kwaśny, F.A. Sala, M.A. Karpierz, N.F. Smyth and G. Assanto, "Curved optical solitons subject to transverse acceleration in reorientational soft matter," *Nature Scien. Reports,* **7**, 12385 (2017).

[48] F.A. Sala, N.F. Smyth, U.A. Laudyn, M.A. Karpierz, A.A. Minzoni and G. Assanto, "Bending reorientational solitons with modulated alignment," *J. Opt. Soc. Amer. B,* **34**, 2459–2466 (2017).

[49] U.A. Laudyn, M. Kwaśny, M. Karpierz, N.F. Smyth and G. Assanto, "Accelerated optical solitons in reorientational media with transverse invariance and longitudinally modulated birefringence," *Phys. Rev. A,* **98**, 023810 (2018).

[50] G.A. El, V.V. Geogjaev, A.V. Gurevich and A.L. Krylov, "Decay of an initial discontinuity in the defocusing NLS hydrodynamics," *Physica D,* **87**, 186–192 (1995).

[51] F.W. Dabby and J.R. Whinnery, "Thermal self-focusing of laser beams in lead glasses," *Appl. Phys. Lett.,* **13**, 284–286 (1986).

[52] E.A. Kuznetsov and A.M. Rubenchik, "Soliton stabilization in plasmas and hydrodynamics," *Phys. Rep.,* **142**, 103–165 (1986).

[53] N. Ghofraniha, C. Conti, G. Ruocco and S. Trillo, "Shocks in nonlocal media," *Phys. Rev. Lett.,* **99**, 043903 (2007).

[54] C. Rotschild, M. Segev, Z. Xu, Y.V. Kartashov and L. Torner, "Two-dimensional multipole solitons in nonlocal nonlinear media," *Opt. Lett.,* **31**, 3312–3314 (2006).

[55] C. Rotschild, B. Alfassi, O. Cohen and M. Segev, "Long-range interactions between optical solitons," *Nature Phys.,* **2**, 769–774 (2006).

[56] M. Segev, B. Crosignani, A. Yariv and B. Fischer, "Spatial solitons in photorefractive media," *Phys. Rev. Lett.,* **68**, 923–926 (1992).

[57] A. Cheskidov, D.D. Holm, E. Olson and E.S. Titi, "On a Leray-α model of turbulence," *Proc. R. Soc. Lond. A,* **461**, 629–649 (2005).

[58] R. Penrose, "Quantum computation, entanglement and state reduction," *Phil. Trans. R. Soc. Lond. A,* **356**, 1927–1939 (1998).

[59] B. Fornberg and G.B. Whitham, "Numerical and theoretical study of certain non-linear wave phenomena," *Phil. Trans. Roy. Soc. Lond. Ser. A— Math. and Phys. Sci.,* **289**, 373–404 (1978).

[60] T.P. Horikis, "Small-amplitude defocusing nematicons," *J. Phys. A,* **48**, 02FT01 (2015).

[61] T.F. Chan and T. Kerkhoven, "Fourier methods with extended stability intervals for KdV," *SIAM J. Numer. Anal.,* **22**, 441–454 (1985).

[62] L.N. Trefethen, *Spectral Methods in MATLAB*, SIAM, Philadephia (2000).

[63] I.M. Gelfand and S.V. Fomin, *Calculus of Variations,* Prentice-Hall, Englewood Cliffs, New Jersey (1963).

[64] T.R. Marchant and N.F. Smyth, "An undular bore solution for the higher-order Korteweg-de Vries equation," *J. Phys. A: Math. Gen.,* **39**, L563–569 (2006).

[65] M. Peccianti, C. Conti and G. Assanto, "Observation of optical modulational instability in a non-local medium," *Phys. Rev. E,* **68**, 025602(R) (2003).

[66] G. Assanto, M. Peccianti and C. Conti, "One dimensional transverse modulational instability in nonlocal media with a reorientational nonlinearity," *IEEE J. Sel. Top. Quantum Electron.,* **10**, 862–869 (2003).

[67] M. Van Dyke, *An Album of Fluid Motion,* Parabolic Press, Stanford, California (1982).

[68] G.A. El, E.G. Khamis and A. Tovbis, "Dam break problem for the focusing nonlinear Schrödinger equation and the generation of rogue waves," *Nonlinearity,* **29**, 2798–2836 (2016).

[69] T.R. Marchant and N.F. Smyth, "Approximate techniques for dispersive shock waves in nonlinear media," *J. Nonlin. Opt. Phys. Mater.,* **21**, 1250035 (2012).

[70] R.H.J. Grimshaw and N.F. Smyth, "Resonant flow of a stratified fluid over topography," *J. Fluid Mech.,* **169**, 429–464 (1986).

[71] T.R. Marchant, "Asymptotic solitons of the extended Korteweg-de Vries equation," *Phys. Rev. E,* **59**, 3745–3748 (1999).

[72] T.R. Marchant and N.F. Smyth, "Initial-boundary value problems for the Korteweg-de Vries equation", *IMA J. Appl. Math.,* **47**, 247–264 (1991).

[73] T.R. Marchant and N.F. Smyth, "The initial-boundary problem for the Korteweg-de Vries equation on the negative quarter-plane," *Proc. Roy. Soc. London A,* **458**, 857–871 (2002).

[74] A. Moro and S. Trillo, "Mechanism of wave breaking from a vacuum point in the defocusing nonlinear Schrödinger equation," *Phys. Rev. E,* **89**, 023202 (2014).

[75] R.F. Bikbaev, "Finite-gap attractors and transition processes of the shock-wave type in integrable systems," *J. Math. Sci.,* **77**, 3033–3041 (1995).